117 (2023) 205053

Contents lists available at ScienceDirect

Gas Science and Engineering

journal homepage: www.journals.elsevier.com/gas-science-and-engineering

Ultra-long-distance transport of supercritical natural gas (SNG) at very-high mass flow rates via pipelines through land, underground, water bodies, and ocean

Vish Prasad [a,*], Laura M. Almara [a], Guo-Xiang Wang [b]

[a] University of North Texas, Department of Mechanical Engineering, UNT Discovery Park, Denton, TX, 76207-7102, USA
[b] The University of Akron, Department of Mechanical Engineering, Akron, OH, 44325, USA

ARTICLE INFO

Keywords:
Anomalous state
Dense phase
Joule-thomson effect
Pipeline under ocean
Pumping power
Compression station

ABSTRACT

A detailed study of SNG transport using a computational model that accounts for compressibility and Joule-Thomson effects is presented, for the first time. It shows that the transport distance and mass flow rate of supercritical natural gas (SNG) - above the cricondenbar and cricondentherm, and beyond the anomalous state - can exceed far beyond that achieved or proposed under high pressure, dense phase conditions, thus far. As an example, SNG (average composition of USA/Canada gas), at 800 kg/s can travel, without recompression, to 4801 km. It is revealed that the pressure-drop and pumping power per unit length decrease asymptotically as the inlet pressure increases beyond 20 MPa; orders-of-magnitude lower than that at low pressures. The increase in inlet pressure, pipe diameter, and/or heat conductance of the pipe wall increases the distance travelled by SNG whereas the increase in mass flow rate and surrounding temperature has a negative effect, including the strengthening of Joule-Thomson cooling near the exit. SNG pipelines at ocean bottom offer many advantages, including shorter distances, isothermal flows (~4 °C), and balance between the outer and inner pressures. Also, SNG delivery at 6 MPa can allow regional distribution without immediate recompression. SNG pipelines therefore offer enormous possibilities of energy-efficient transport of natural gas to far-distant intra- and inter-continental destinations, not feasible thus far, which is urgently needed for uninterrupted supply of natural gas and worldwide energy security.

1. Introduction

The most crucial part of the natural gas delivery system is its transport from the processing facilities to distribution centers, since the gas is found and extracted only in few places within a producer country but needs to be distributed throughout the country. In addition, most countries do not have natural gas reserves and even if they have the reserves those reserves cannot meet their demands. That means, trans-border pipelines are needed to deliver natural gas to non-producing and not-sufficiently-producing countries. Such pipelines do exist in many parts of the world. However, the complexity of terrain (hills and mountains), climate conditions, unfavorable relationship among or between the producing, transit, and consuming countries, and/or ocean separating the exporting and importing countries have inhibited the construction of cross-country and inter-continental long-distance pipelines (Mokhatab et al., 2019; Molnar, 2022).

One solution that is commonly used to transport natural gas, when the pipeline delivery is not feasible, is to liquefy the gas and transport it across the countries as well as internationally via large tankers. The challenge with LNG is that the natural gas needs to be cooled to about −160 °C and be maintained at that temperature all along the transit, i.e., requiring cooling while being transported. The cost of LNG involves: (i) investment in building cooling plants and their operational costs, (ii) tankers with cooling systems and continuous energy demand, (iii) transportation cost and port fees, (iv) delays due to weather conditions, (v) security against piracy and hostile countries enroute, (vi) regasification at delivery sites, and (vii) environmental cost of transportation via road, rail, and/or ocean, as the case may be. Consequently, the cost of LNG is higher than the cost of natural gas delivered by pipelines, even if the environmental impact is not accounted for (Mokhatab et al., 2019; Molnar, 2022). Moreover, it is forecasted that there will be a huge gap between the demand of LNG and the worldwide capacity to produce it

* Corresponding author.
E-mail address: vish.prasad@unt.edu (V. Prasad).

https://doi.org/10.1016/j.jgsce.2023.205053
Received 12 February 2023; Received in revised form 22 May 2023; Accepted 26 June 2023
Available online 12 July 2023

(Chestney, 2022).

Since 1970, there have been efforts to design high-pressure pipelines to transport natural gas - long distances, at high mass flow rates - under the dense phase conditions (Katz and King, 1970; King, 1991, 1992; King et al., 2002; Mazurek and Anderson, 1994; Vargas-Vera et al., 2020). Wang and Economides reported, in 2009, that the onshore pipeline operating pressure could be between 4.8 and 7.6 MPa, may be some as high as 27.6 MPa. NaturalGas.org (2023) and Molnar (2022) report the pressure range of 1.38–10.34 MPa and 1.5–12 MPa, respectively; the inlet pressure of Nord Stream 1 (NS1) is reported to be 22 MPa (Beaubouef, 2011). To the authors' knowledge, a few projects where high-pressure natural gas pipelines may be experiencing dense phase are: Asgard field, Norwegian sea; Offshore Associated Project, UAE; NS1 (Russia to Germany; Moshfeghian et al., 2022); and Iran's fourth national pipeline (Zivdar and Abofarakh, 2021), see Almara et al. (2023) for a brief summary.

Recently, we have demonstrated that several of the assumptions regarding dense phase are questionable (Almara et al., 2023). In addition, the dense phase as measured by its pressure above the cricondenbar does not guarantee that a mixture of gases, e.g., natural gas with various hydrocarbons and non-hydrocarbons as its constituents, will be devoid of thermophysical property-related complexities during its transit. This is because the cricondenbar and cricondentherm lie within the anomalous state, which is characterized by large-scale variations in thermophysical properties, flow and thermal instabilities/oscillations, and complexities in heat transfer. Indeed, the most preferred conditions for the transport of supercritical natural gas (SNG) are: above the critical pressure and critical temperature, above the cricondenbar and cricondentherm, and beyond the anomalous state (Prasad et al., 2022c; Almara et al., 2023).

For methane, such conditions exist at pressure, $P > 5$ MPa and temperature, $T >$ - 30 °C whereas based upon the average composition of natural gases from US/Canada, West Asia, and North Sea, $P \geq 6$ MPa and $T > -30$ °C may be appropriate/safe for SNG transport. Corresponding gray zones, which will require special design considerations are also identified. Reduced pressure, P_r, of 1.15 and temperature, T_r, of 1.25 and 1.4 may be appropriate to delimit the Unsafe Zone/Gray Zone and Gray Zone/Safe zone. It is also shown that the critical temperature, cricondentherm, and anomalous region can be moved to lower temperatures by adding one or more modifier gases with low T_c, e.g., methane, nitrogen, and argon; or, higher using gases with high T_c, such as ethane, propane, and carbon dioxide (Prasad et al., 2022c; Almara et al., 2023). Our main goal here is to investigate SNG transport using a physics-based computational model. Following is a short summary of the development of theoretical models for transport of gases.

Historically, Issa and Spalding (1972) were the first to treat numerically the unsteady one-dimensional compressible flow in pipes, focusing on the hyperbolic behavior of high-speed compressible flows together with friction and heat transfer. This approach was later used by MacLaren et al. (1975) to model various 1D compressible flows in pipes, e.g., in a reciprocating compressible system. These early works, however, dealt with only ideal gases.

In 1981, Goldwater and Fincham presented a complete set of equations for 1D compressible flow in natural gas pipelines, which incorporated both friction and heat transfer with the pipe wall and the environment. The equations were derived based on the conservation laws of mass, momentum, and energy; the energy equation was written in terms of enthalpy of the gas. van Deen and Reintsema (1983) then introduced the equation of state (EOS) for real gases, and converted the original equations to those based on the pressure, velocity, and temperature as dependent variables. They solved these equations to simulate the dynamics of natural gas pipelines of Gasunie, Netherlands, for pressures up to 6.6 MPa and length of 400 km. In order to simplify the treatment of the energy equation, they assumed the friction factor as a constant and used a linear relation between the temperature and pressure along the flow. A detailed review of both numerical and experimental research on flow dynamics of dense natural gases in high-pressure pipelines, up to 1987, was reported by Thorley and Tiley (1987).

The above studies indicated that for the design and operation of offshore natural gas pipelines, steady-state solutions of gas flow were sufficient. Various analytical solutions that relate the gas flow rate with pressure drops were developed using simplified isothermal models, and generally, a constant friction factor. Analytical expressions for variation of gas temperature along the pipeline have also been developed and used in the industry (Schorre, 1954; Coulter and Bardon, 1979).

Ouyang and Aziz (1996) were probably the first to investigate systematically the effects of various processing parameters on steady-state flow in natural gas pipelines by comparing the numerical solutions to the ones from the simplified correlations. In particular, they examined more than a dozen of correlations for the prediction of friction factor, and the effect of the surface roughness and gas viscosity. The model predictions were compared with the measured data. Abdolahi et al. (2007) further extended this steady-state model by incorporating the latest EOS to calculate more accurately the properties of the gas.

Later, in a series of papers, Chaczykowski and co-workers (Osiadacz and Chaczykowski, 2001; Chaczykowski, 2009, 2010) examined the effect of heat transfer on natural gas flow, with pressures up to 8.4 MPa, for both steady state and transient conditions. They noticed that both the heat transfer between the gas and the environment and the Joule-Thomson effect due to pressure drop lead to significant temperature variation along the pipelines. These authors also studied the effect of various equations of state to calculate the properties of the natural gas. They found that the simple 3-parameter cubic EOS can make accurate predictions of the properties in the pressure range considered by them. Moreover, they observed that the accurate predictions of friction factor and overall heat transfer coefficient were both critical to the steady-state and transient modeling of natural gas flows in high-pressure pipelines.

In 2008, Langelandsvik carried out experimental measurements of the surface roughness of commercial pipes and correlated them with the model predictions, which led to a new equation for friction factor. Langelandsvik also examined the approximations introduced by one-dimensional uniform flow assumption to treat the pipeline flow. He rederived the momentum and energy equations in 1D form by averaging the three-dimensional forms with turbulence, over the cross-section of the pipe, and showed that the 1D compressible flow model derived from the differential element of the pipe is consistent with the 1D average of the intrinsic 3D flow. Ramsen et al. (2009), on the other hand, carried out a numerical analysis of heat transfer between the gas inside the pipe and the environment for both the buried pipelines and the pipelines at the bottom of the ocean, and examined the effect of overall heat transfer coefficient.

A detailed analysis of the flow and heat transfer of high-pressure natural gas in large diameter pipes under dense phase conditions was carried out by Helgaker (2013, 2014a, 2014b) using Langelandsvik equations. Their model included the newly developed friction factor. The authors examined systematically the effect of the parameters used in these correlations as well as the appropriateness of various EOSs to predict the properties. The finding was that the improvement in property predictions using more sophisticated EOSs was marginal. In addition, a transient heat conduction model was employed for buried pipelines whose results indicated that the steady-state heat transfer might be sufficiently accurate.

Here, we present a robust method by which supercritical (SC) gases and their mixtures, in particular the natural gas, can be transported at very-high mass flow rates, without recompression, to destinations that are thousands of kilometers away. A major condition to achieving this is that the gas remains under the safe SC conditions, in terms of pressure and temperature, from the inlet to the exit (Almara et al., 2023; Prasad et al., 2022c). We employ the steady-state form of the computational model of Langelandsvik (2008) and Helgaker (2013) to perform the flow

simulations for varying inlet pressure, mass flow rate, pipe diameter, surrounding temperature, overall heat transfer coefficient between the gas and the surrounding, and cooling due to gas expansion (Joule--Thomson effect). The mechanisms that make transport of fluid at SC conditions far more effective and pumping power-efficient than that at low and moderately high pressures are analyzed for major governing parameters. In addition, we examine the benefits of SNG pipelines laid at the bottom of the ocean, where the condition is isothermal, ~4 °C. We also explore the possibility of local/regional distribution of delivered SNG without immediate recompression, since the gas pressure at delivery point would be 6 MPa (6000 kPa), or higher.

2. Theroretical model and methodology for calculations

We employ here the steady-state version of the model of Langelandsvik (2008) and Helgaker (2013) to investigate the variations of flow and heat transfer in natural gas pipelines under supercritical conditions. The model accounts for both compressibility and Joule-Thomson effects as well as the thermophysical property variations. We consider the pressures and temperatures in the Safe Zone, where the property variations are monotonic and no anomalous behavior is expected. Under these conditions, the applicability of 1D compressible turbulent model (Langelandsvik, 2008; Ramsen et al., 2009; Helgaker, 2013) is certainly acceptable. Here, we will adopt the relationships for friction factor, viscosity, and thermal conductivity of natural gas as proposed in the above works. Additionally, as outlined in Almara et al. (2023), the Peng-Robinson (PR) cubic equation of state is used to determine the thermodynamic properties (Peng and Robinson, 1976).

2.1. Governing equations and transport calculations

The steady-state form of the governing equations for one-dimensional compressible, turbulent flow along a constant diameter pipe (x-direction) are (Helgaker, 2013):

$$\frac{\partial(\rho u)}{\partial x}=0 \tag{1}$$

$$\frac{\partial(\rho u^2+P)}{\partial x}=-\frac{f\rho|u|u}{2D}-\rho g\sin\theta \tag{2}$$

$$\rho c_v\left(u\frac{\partial T}{\partial x}\right)+T\left(\frac{\partial P}{\partial T}\right)_\rho\frac{\partial u}{\partial x}=\frac{f\rho u^3}{2D}-\frac{4U}{D}(T-T_a) \tag{3}$$

Here, the friction factor, f, is related to the wall shear stress (τ_w) between the gas and pipe wall,

$$f=\frac{4\tau_w}{\frac{1}{2}\rho u^2}=-\frac{\partial p}{\partial x}\frac{2D}{\rho u^2} \tag{4}$$

and the total heat transfer coefficient, U, between the gas and the surroundings is determined by,

$$U=\frac{q_w'}{\pi D(T-T_a)} \tag{5}$$

where q_w' is the rate of heat transfer per unit length of the pipe. To simplify the treatment at this stage, U has been taken as a constant throughout the pipe length.

It is to be noted that the second term of the left side of energy equation, Eq. (3), represents the Joule-Thomson effect which accounts for the cooling upon expansion. A rigorous EOS of the real gas, $P=P(T,\rho)$, is therefore essential to estimate accurately this term. As noted earlier, we have employed the Peng-Robinson equation of state together with other required thermodynamic properties in the equation such as density, ρ, and specific heat at constant volume, c_v.

In solving Eqs. (1)–(3), the mass flow rate $\dot{m}=\rho u(\pi D^2/4)$ is considered constant along the entire length of pipeline. Replacing the mean velocity, $u(x)$, by $\dot{m}$, the above equations for $\theta=0$ (horizontal pipe) can be reduced to the following two first-order ordinary differential equations for pressure $P(x)$ and temperature $T(x)$ along the pipe,

$$\frac{dP}{dx}=\frac{2BD}{\rho^2}\frac{d\rho}{dx}-\frac{B}{\rho}f \tag{6}$$

$$\frac{dT}{dx}=\frac{T}{\rho^2 c_v}\left(\frac{\partial P}{\partial T}\right)_\rho\left(\frac{d\rho}{dx}\right)+\frac{Bf}{\rho^2 c_v}-\frac{\pi DU}{c_v\dot{m}}(T-T_a) \tag{7}$$

where the constant mass flow parameter, B, is defined as,

$$B=\frac{8\dot{m}^2}{\pi^2 D^5} \tag{8}$$

Since the density of the gas is a function of pressure $P(x)$ and temperature $T(x)$,

$$\frac{d\rho}{dx}=\left(\frac{\partial\rho}{\partial P}\right)_T\frac{dP}{dx}+\left(\frac{\partial\rho}{\partial T}\right)_P\frac{dT}{dx}=\rho\kappa\frac{dP}{dx}-\rho\beta\frac{dT}{dx} \tag{9}$$

where κ is the isothermal compressibility and β is the thermal expansion coefficient of the gas:

$$\kappa=\frac{1}{\rho}\left(\frac{\partial\rho}{\partial P}\right)_T,\ \beta=-\frac{1}{\rho}\left(\frac{\partial\rho}{\partial T}\right)_P \tag{10}$$

Substituting Eqs. (9) and (10) into Eqs. (6) and (7) leads to,

$$\left(1-\frac{2BD}{\rho}\kappa\right)\frac{dP}{dx}=-\frac{B}{\rho}f-\frac{2BD}{\rho}\beta\frac{dT}{dx} \tag{11}$$

$$\left[1-\frac{T\beta^2}{\rho c_v\kappa}\right]\frac{dT}{dx}=+\frac{Bf}{\rho^2 c_v}-\frac{\pi DU}{c_v\dot{m}}(T-T_a)+\frac{T\beta^2}{\rho c_v\kappa}\frac{dP}{dx} \tag{12}$$

where we have also used the identity,

$$\left(\frac{\partial P}{\partial T}\right)_\rho=\frac{\beta}{\kappa} \tag{13}$$

It is important to note that Eqs. (11) and (12) are valid in all regimes of single phase as long as the flow is predominantly one-dimensional, no large-scale changes and/or inversions in properties occur, and no thermal instabilities/oscillations are expected. Consequently, Eqs. (11) and (12) can be used to model the flow from its subcritical gaseous state to the supercritical fluid state as long as the gas does not encounter the anomalous region. Furthermore, Eqs. (11) and (12) can be reduced to an isothermal flow when the second term on the right-hand side are ignored. On the other hand, if the compressibility effect is very weak, the contribution of second term on the left side of Eq. (11) will vanish.

The friction factor, f, is traditionally calculated using the Colebrook-White correlation,

$$\frac{1}{\sqrt{f}}=-2\log\left(\frac{\varepsilon}{3.7D}+\frac{2.51}{\mathrm{Re}\sqrt{f}}\right) \tag{14}$$

where ε is the surface roughness of the pipe and Re is the Reynolds number defined as,

$$\mathrm{Re}=\frac{\rho uD}{\mu}=\frac{\rho D}{\mu}\frac{4\dot{m}}{\rho\pi D^2}=\frac{4\dot{m}}{\pi D\mu} \tag{15}$$

However, for natural gas pipeline calculations, the European Gas Research Group (GERG) suggest to use the following correlation,

$$\frac{1}{\sqrt{f}}=-\frac{2}{n}\log\left[\left(\frac{\varepsilon}{3.7D}\right)^n+\left(\frac{1.499}{dr\cdot\mathrm{Re}\sqrt{f}}\right)^{0.942n\cdot dr}\right] \tag{16}$$

where dr is the draught factor which accounts for the pressure losses due to curvature and fittings in the pipeline. In this GERG correlation, n is used to control the shape of transition from Reynolds number-

dominated flow to surface roughness flow. Sletfjerding et al. (1998) suggested $n = 3$ and $dr = 1.01$ based on their experimental data.

The Lee-Gonzales-Eakin correlation (Lee et al., 1966) is used to determine the viscosity of high-pressure natural gas,

$$\mu = Ke^{X\rho^Y} \tag{17}$$

with

$$K = \frac{(9.379 + 0.0161M)(9T/5)^{1.5}}{209.2 + 19.26M + 9T/5} \quad X = 3.448 + \frac{986.4}{9T/5} + 0.0101M$$
$$Y = 2.447 - 0.2224X \tag{18}$$

The numerical coefficients in the relations for K, X, and Y have been modified by Langelandsvik (2008) from the original Lee formula, based on their experimental data (Lee et al., 1966).

Equations (11) and (12) can be solved by an implicit finite-difference method, marching along the pipe (x-direction). For given inlet and outlet pressures of the gas, the above model can then predict the following quantities: (a) the transmission distance, L, (b) the gas flow conditions, $P(x)$ and $T(x)$, (c) local pressure gradient, dP/dx, (d) local pumping power, dW/dx, as

$$\frac{d\dot{W}}{dx} = \frac{\dot{m}}{\rho}\frac{dP}{dx} \tag{19}$$

and (e) total power consumption, $\dot{W}(x)$, from the inlet ($x = 0$) of the pipe to any distance x along the pipe

$$\dot{W}(x) = \int_0^{\dot{W}(x)} \delta\dot{W} = \dot{m}\int_0^x \frac{1}{\rho}\left(\frac{dP}{dx}\right)dx \tag{20}$$

The input parameters are: pipe diameter, D, mass flow rate, $\dot{m}$, gas composition, z_i, inlet and outlet gas pressures, P_i, and P_o, respectively, inlet gas temperature, T_i, outside/ambient temperature, T_a, and overall heat transfer coefficient (heat conductance) across the pipe layers, U. Here, U may include the convective heat transfer at inner and outer surfaces, and conduction through the pipe wall that may consist of coatings at one or both surfaces, pipe material, and insulation. In the present paper, the four thermodynamic properties of the gas involved in Eqs. (11) and (12), i.e., ρ, β, κ, and c_v, are obtained using the PR EOS. Note that we have developed our own software based on the above equations/descriptions to perform the simulations presented here.

Fig. 1(a)-(c) present validation of the use of Peng-Robinson EOS for thermophysical properties and the computational scheme for flow quantities. Fig. 1(a) and (b) show very good agreement between our predictions for density and specific heat and that obtained from the current version of REFPROP (Lemon et al., 2018). Fig. 1(c), on the other hand shows a comparison between our predictions and that reported by Vargas-Vera et al. (2020) for the pipe flow of a natural gas under dense phase conditions. An excellent match between the two results has been obtained for the variation of gas pressure along the pipe for $P_i = 15$ MPa and $P_o = 12$ MPa over a pipe length of 285 km.

2.2. Governing parameters and select natural gas compositions

We have used data reported in the literature to select the range of major governing parameters. For example, the pipe diameter for long-distance transport of processed gas is reported to be 20–42 in (0.51–1.061 m) by Wang and Economides (2009), 16–48 in (0.41–1.22 m) by NaturalGas.org (2023), 16–56 in (0.41–1.42 m) by Molnar (2022), and 1.153 m by Moshfeghian et al. (2022) for NS1. As per Nord Stream AG (2023), the total mass flow rate of two NS1 pipelines is 110 billion m^3 per year, that is equivalent to ~620 kg/s per pipeline. Moshfeghian et al. (2022) reports this to be 647.7 kg/s. The pressure ranges reported by NaturalGas.org and Molnar are 1.38–10.34 MPa and 1.5–12 MPa, respectively. Wang and Economides (2009), on the other hand, state that the onshore pipeline operating pressure is about 700 to 1100 psi

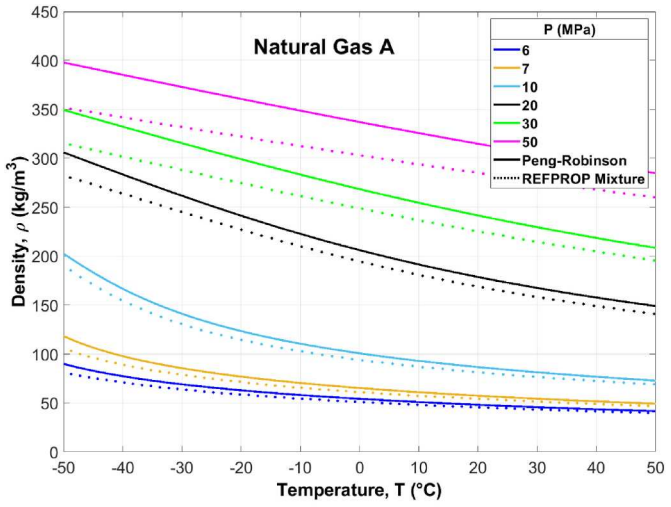

(a)

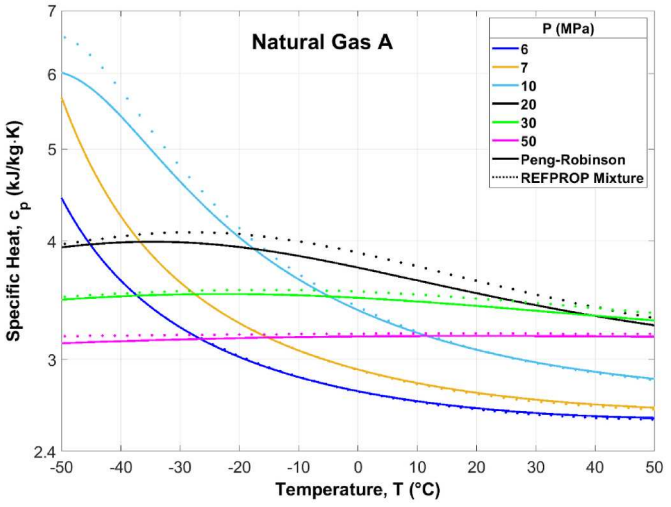

(b)

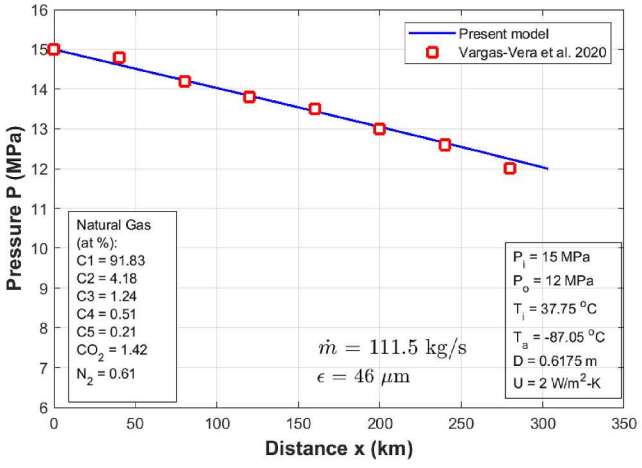

(c)

Fig. 1. Comparison of (a) density and (b) specific heat predictions by Peng-Robinson EOS and REFPROP (Lemmon et al., 2018) (c) calculated pressure vs distance (L = 285 km) by the present model with that of Vargas-Vera et al. (2020).

(4.8–7.6 MPa) with some as high as 4000 psi (27.6 MPa).

Although not confirmed, the inlet pressure of NS1 is reported to be 22 MPa (Beaubouef, 2011). Since our goal is to demonstrate the enormous potential of natural gas transport under SC conditions, we have considered the range of pipe diameter, D, as 0.6–1.5 m, mass flow rate, $\dot{m}$, as 300–1200 kg/s, and inlet pressure, P_i, as high as 30 MPa (Table 1). To keep the gas within the safe zone (beyond anomalous state) from inlet to exit, the outlet pressure, P_o has been taken as 6 MPa (Almara et al., 2023). In choosing these parameters, we are also guided by the "dream" of King et al. (2002), who presented the idea of super high pressure, dense phase arctic pipeline of up to 54 in (1.37 m) with 42.5 MPa inlet pressure. Note that P_i of 30 MPA is not unreasonable from the pipeline materials point of view. For example, ultimate tensile and yield strengths of austenitic steel are 515 and 205 MPa (Material-properties.org, 2023) and that of X120, Grade 825 are 931 and 827 MPa, respectively (Corbett et al., 2004; Yoo et al., 2011; Witek, 2015). Moreover, much stronger materials can be developed if the presently available materials cannot meet the requirements.

In general, the surface roughness, ε, can vary from 2 to 15 μm (Langelandsvik, 2008; Langelandsvik et al., 2008). However, it reduces significantly with appropriate coatings on inside of the pipe, hence we have taken it as 5 μm () except when the effect of the roughness is examined. The surrounding temperature of −30 °C–30 °C is considered keeping in mind the temperatures of the North Sea/Polar region and West Asia as well as that for the Safe Zone (Almara et al., 2023). Heat conductance, U, of 2 W/m^2·K represents strong thermal resistance whereas 100 W/m^2·K implies very low resistance to heat transfer between the flowing gas and the surrounding (Helgaker, 2013). As seen later, in comparison to surrounding temperature and heat conductance, the inlet temperature has weaker effect, particularly on the long-distance pipeline and therefore 4–10 °C range may suffice for the present simulation. Here, consideration of 4 °C is guided by the temperature of the ocean bottom, In presenting our results, we consider both the transmission distances and mass flow rates 25% above the current state-of-the-art pipeline, NS1 (~1200 km, ~620 kg/s), as ultra-long transmission distances and very-high mass flow rates, i.e., L > 1600 km and $\dot{m}$ >800 kg/s.

3. Results and discussions

Here, we first consider a pipe with $\varepsilon = 5$ μm and look at the effect of high inlet pressure, which is well into the supercritical regime, $P = 20$, 25, and 30 MPa. This gives us some baseline cases to examine the effects of mass flow rate, pipe diameter, variation in gas composition, surface roughness, heat conductance, inlet and surrounding temperatures, and so on. As appropriate, we discuss the pressure and temperature variations along the pipeline. Lastly, we present the advantages of using SNG pipelines at the ocean bottom as well as the possibility of regional transport beyond the delivery point, without immediate recompression.

3.1. Effect of inlet pressure and mass flow rate

Fig. 2(a) shows that when Gas A (Table 2) with mass flow rate of $\dot{m}$ = 800 kg/s, and temperature, $T_i = 10$ °C, enters a pipe of 1 m diameter at 20 MPa and exits at 6 MPa, it can travel 467 km; the heat conductance,

Table 1
Variables for present calculations.

Pipe diameter, D	0.6–1.5 m
Mass flow rate,$\dot{m}$	300-1200 kg/s
Inlet pressure, P_i	20–30 MPa
Inlet temperature, T_i	4°C–10 °C
Outlet pressure, P_o	6 MPa
Surrounding temperature, T_a	−30 °C – 30 °C
Overall heat conductance across the pipe layers, U	2–100 W/m^2·K
Surface roughness, ε	0–15 μm

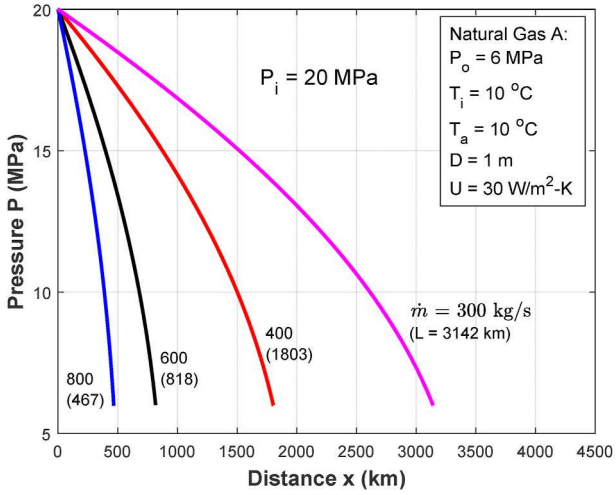

(a)

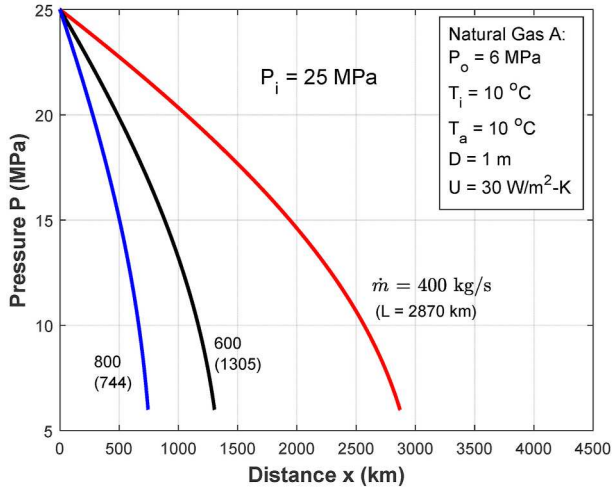

(b)

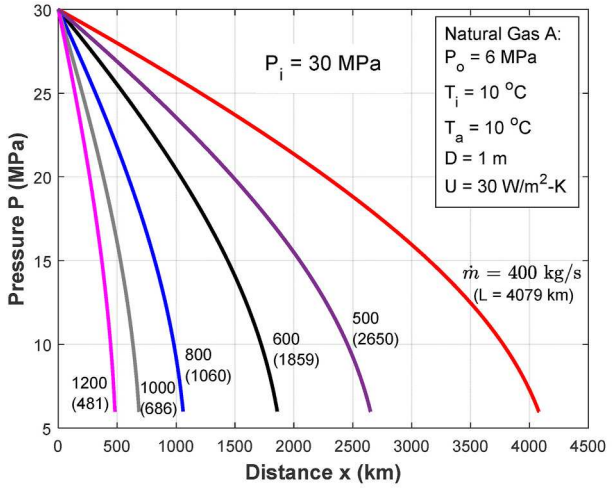

(c)

Fig. 2. Transmission distance for supercritical **natural** gas (SNG), Gas A when the inlet pressure, P_i, is (a) 20 MPa, (b) 25 MPA, and (c) 30 MPa, and outlet pressure is 6 MPa, for a range of mass flow rate, $\dot{m}$, with pipe diameter, $D = 1$ m, surface roughness, $\varepsilon = 5$ μm, inlet temperature, $T_i = 10$ °C, surrounding temperature, $T_a = 10$ °C, and heat transfer coefficient of the pipe between its inner and outer surfaces, $U = 30$ W/m^2·K.

Table 2
Constituents and compositions of selected natural gas and their critical points (P_c, T_c) and criconden conditions (P_{cr}, T_{cr}).

Components	P_c, MPa	T_c, °C	Gas A[1]	Gas B[2]	Gas C[3]
N_2 (Nitrogen)	3.39	−146.96	0.50	1.62	0.700
CO_2 (Carbon Dioxide)	7.38	30.98	0.30	0.70	2.222
C1 (CH_4, Methane)	4.60	−82.59	94.73	94.90	89.160
C2 (C_2H_6, Ethane)	4.88	32.18	4.20	2.50	7.350
C3 (C_3H_8, Propane)	4.25	92.68	0.20	0.20	0.510
i-C4 ($C_4H_{10,}$ i-Butane)	3.65	134.66	0.02	0.03	0.030
n-C4 (C_4H_{10}, n-Butane	3.80	151.98	0.02	0.03	0.024
i-C5 (C_5H_{12}, i-Pentane)	3.38	187.25	0.015	0.01	0.001
n-C5 (C_5H_{12}, n-Pentane)	3.37	196.60	0.015	0.01	0.003
Total			100	100	100
Critical Temperature, T_c (°C, K)			−73.25, 199.9	−77.15, 196.0	−66.85, 206.3
Cricondentherm, T_{cr} (°C, K)			−66.90, 206.25	−70.92, 202.23	−58.15, 215.0
Critical Pressure, P_c (MPa)			5.23	5.04	5.612
Cricondenbar, P_{cr} (MPa)			5.35	5.189	5.908

1-US and Canada, 2-West Asia, and 3-North Sea (Averages).

U, between the gas inside the pipe and the surrounding at $T_a = 10$ °C is taken as 30 W/m^2·K. In this case, the pressure drop per unit length is very rapid, ~30 kPa/km (or 30 Pa/m). However, if the mass flow rate is reduced to 600 kg/s, the distance travelled increases to 818 km. The corresponding delivery distances for 400 and 300 kg/s are 1803 and 3142 km (1120 and 1952 miles), respectively. Similar reduction in distance with increasing mass flow rate has also been reported by Baker (2005). Note that the change in transmission distance for the same reduction in mass flow rate, i.e., 200 kg/s, is not the same and indicates a non-linear relationship between the mass flow rate and transmission distance.

As is well known the lower the mass flow rate, the longer is the distance travelled. However, without recompression 3142 km or even 1803 km would be very long distances for natural gas delivery. This would be possible if the gas is maintained all along the pipe, from inlet to exit, at a supercritical pressure, 6 MPa $< P <$ 20 MPa (6 MPa $> P_{cr} > P_c$); the temperature in this case is far above T_c (= −73.25 °C) and T_{cr} (= −66.90 °C), and indeed, is out of the anomalous region (Almara et al., 2023).

If the inlet pressure is increased to 25 MPa (Fig. 2(b)), the distance travelled for 400 kg/s increases from 1803 km at 20 MPa to 2870 km; an increase of almost 60%. A similar increase of 60% in delivery distance takes place in the case of 600 kg/s (from 818 to 1305 km), and 800 kg/s (467–744 km). In addition, the pressure drop with respect to distance becomes much more gradual as the pipe length increases with lower mass flow rates.

Further increase is possible by increasing the inlet pressure to 30 MPa (Fig. 2(c)). In this case, Gas A with a mass flow rate of 600 kg/s can reach a distance of 1859 km. For $\dot{m} = 800$, 1,000, and 1200 kg/s the distance travelled would be 1,060, 686, and 481 km, respectively. Indeed, with $P_i = 30$ MPa and $P_o = 6$ MPa, Gas A flowing at 400 kg/s can travel ***4079 km (2534 miles) without recompression***.

Furthermore, a comparison between Fig. 2(a) and (c) reveals that by increasing the inlet pressure by 10 MPa (from 20 to 30 MPa), the transmission distance increases by over ~125% (a factor of ~2.25) and the pressure drop becomes more gradual as the pipe length increases. Note that with the present-day technologies of high strength materials for pipes, it should be possible to achieve 30 MPa pressure for SNG transport. Additionally, the need for very high strength material will go down as the pressure goes down, in the later part of the pipeline. Therefore, we will consider $P_i = 30$ MPa for all other calculations.

3.2. Effect of pipe diameter

The effect of pipe diameter for Gas A is shown in Fig. 3(a)-(c). Fig. 3 (a1) shows that if the diameter of pipe is increased by 20%, from 1 m to 1.2 m, the distance between the inlet and exit increases from 1859 km to 4642 km (2.5 times), when $\dot{m} = 600$ kg/s. Basically, there is a 150% increase in the transmission distance for 44% increase in the cross sectional area. Similarly, 12.66% increase from $D = 1.2$ m–1.35 m brings 80% increase in the distance travelled, from 4642 km to 8338 km. Considering $\dot{m} = 800$ kg/s, Fig. 3(b1) confirms identical diameter effect, 150% increase from $D = 1$ m–1.2 m and 80% increase for $D = 1.2$ m–1.35 m, and similarly, for the mass flow rate of 1000 kg/s in Fig. 3 (c1). That means, the increase in distance travelled with respect to increase in diameter is universal at all mass flow rates as long as the other parameters remain the same, as also shown by Baker (2005).

From Fig. 3(b1) and 3(c1) it is evident that $D > 1.2$ m satisfies our criteria for ultra-long-distance transmission at very-high mass flow rates (Section 2.2), $\dot{m}$ greater than 800 kg/s and L longer than 1600 km. However, there can be many other combinations of mass flow rate and diameter possible if the goal is to achieve either the longest distance or highest mass flow rate. For example, Gas A can travel to 8338 km for $\dot{m} = 600$ kg/s via 1.35 m diameter pipe (Fig. 3(a1)), or to 8114 km for $\dot{m} = 800$ kg/s when $D = 1.5$ m (Fig. 3(b1)). On the other hand, it can travel to 4801 km for $\dot{m} = 800$ kg/s and $D = 1.35$ m (Fig. 3(b1)) or to 5285 km for $\dot{m} = 1000$ kg/s and $D = 1.5$ m (Fig. 3(c1)), and likewise.

Fig. 3(a1)-(c1) supports the observation in Fig. 2(c) that the pressure drops very fast when the distance travelled is less, for all mass flow rates. In Fig. 3(a2)-(c2), the temperature drop shows very similar behavior. Indeed, the temperature goes below the surrounding temperature, T_a, = 10 °C, about −3 °C in Fig. 3(c2) because of the Joule-Thomson effect, to be discussed later. The longer is the transmission distance, the smaller is the variation in gas temperature from the inlet to near-exit, for $T_a \cong T_i$.

3.3. Physics of SC transport: pressure, mass flow rate, and pipe diameter

The pressure, P, as a function of the travel distance x of gas is already presented in Fig. 2(a)–(c) and 3(a1)-(c1), which give us a clear picture of pressure gradient, dP/dx, versus distance. The pressure drop is very rapid when the mass flow rate is high and the distance travelled is short, and vice versa. Obviously, as the inlet pressure increases, the distance travelled increases, and the slope of the curve, dP/dx, decreases. Moreover, the pressure drop is almost linear in the beginning but becomes sharper towards the end (Fig. 2a–c). With the increase in diameter, the distance travelled goes up for a given mass flow rate and the slope, dP/dx, goes down, however, keeping the same trend, almost linear in the beginning and sharper towards the end (Fig. 3(a1)-(c1)).

Now, the dP/dx as a function of pressure is presented in Fig. 4(a) for 40 MPa as the inlet pressure and 1 MPa as the outlet pressure. We have selected these low and high pressures to illustrate the characteristically different behavior of pressure gradients in the subcritical (gaseous, above cricondentherm) and supercritical states. As is evident, the dP/dx for all mass flow rates is very high at low pressures but its slope with respect to pressure starts changing dramatically as the pressure increases, within the subcritical (gaseous) regime, $P < P_c$ (5.23 MPa for Gas A). Indeed, the curves start changing their directions and start becoming asymptotic. Finally, when the pressure goes to some higher values they become almost horizontal, e.g., beyond 15 MPa for $\dot{m} = 400$ kg/s and beyond 25 MPa for $\dot{m} = 1000$ kg/s. This is highly revealing, implying that not only the pressure gradient, dP/dx, decreases from its very high value at 1 MPa to a very low value as the fluid moves towards the critical pressure, but also it achieves almost a constant value at

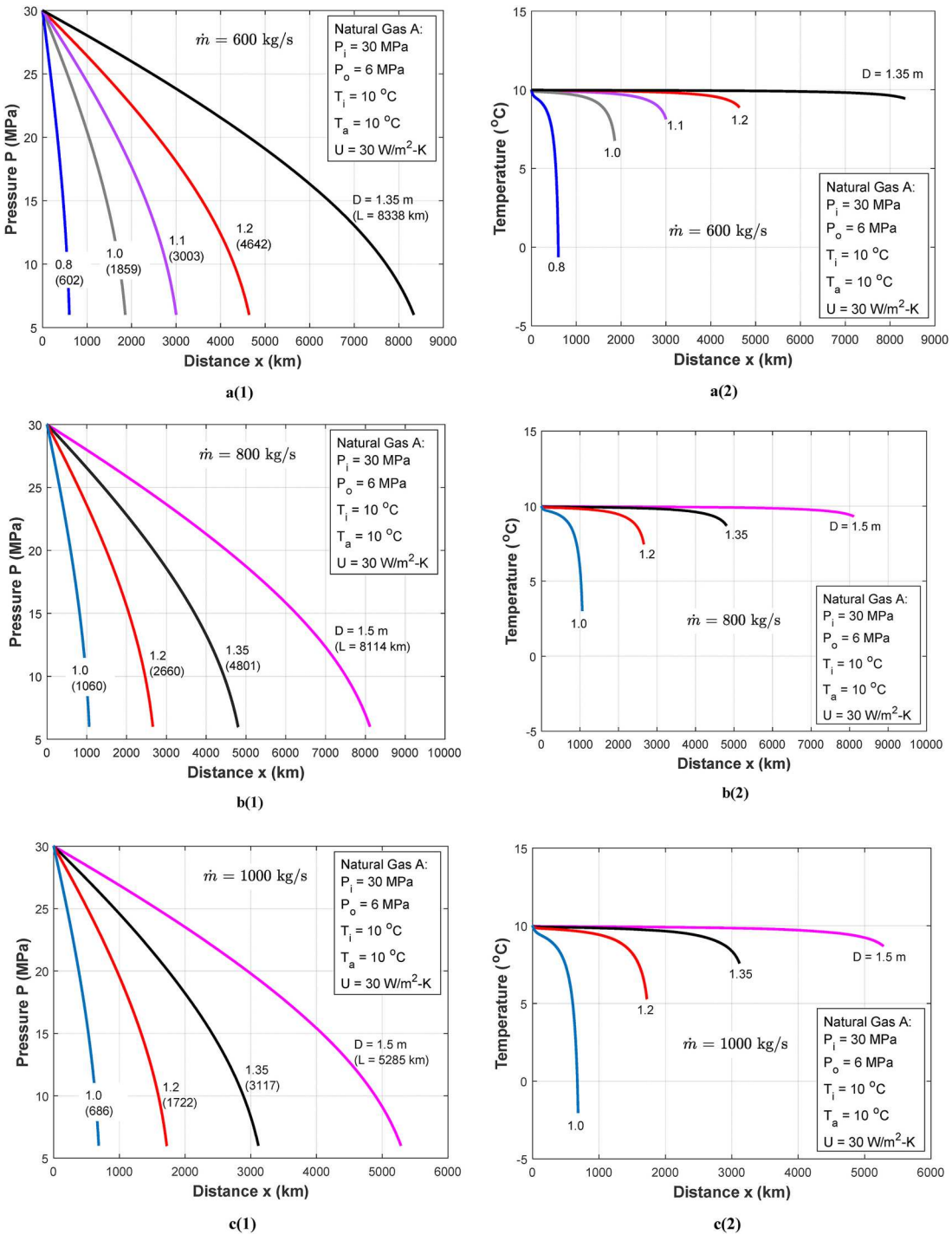

Fig. 3. Transmission distance, pressure drop, and temperature distribution for Gas A for a range of pipe diameter, $D = 0.8$, 1.0, 1.1, 1.2 m, 1.35, and 1.5, with (a1) $\dot{m} = 600$ kg/s, (b1) $\dot{m} = 800$ kg/s, (c1) $\dot{m} = 1000$ kg/s, and (a2-c2) temperature variations.

(high) supercritical pressures. Fig. 4(a) also shows that as the mass flow rate increases, the pressure drops at 1 MPa increases significantly, beyond 150 kPa/km for $\dot{m} > 400$ kg/s. However, all curves change their directions and become asymptotic for $\dot{m} = 400$–1000 kg/s.

Using the pressure gradient, dP/dx, we can now calculate the local power gradient, dW/dx, as a function of pressure, P, using Eq. (19). This is presented in Fig. 4(b), which is again exceedingly revealing; dW/dx decreases substantially from its highest value at 1 MPa to a very low value at 40 MPa. For example, in the case of $\dot{m} = 400$ kg/s, dW/dx of ~7 W/m decreases to ~0.003 W/m. The corresponding reduction for 1000 kg/s is from ~100 W/m to ~0.07 W/m. This, more than three orders-of-magnitude, reduction in power loss per unit length in SC regime is *extraordinarily remarkable* with respect to the SNG transport. Even if we consider the inlet and outlet pressures of 30 and 6 MPa, as considered for most of the simulations presented here, dW/dx decreases from ~0.015 W/m to ~0.005 W/m for $\dot{m} = 400$ kg/s and from ~2 W/m to 0.07 W/m for 1000 kg/s, which is about thirty times reduction in magnitude.

Furthermore, as discussed in the previous section (3.2), the transmission distance increases substantially with the increase in diameter. One of the reasons for this change is that the power required to compensate pressure loss is directly proportional to the pipe diameter, D, (surface area = πDL), whereas the mass flow rate is proportional to

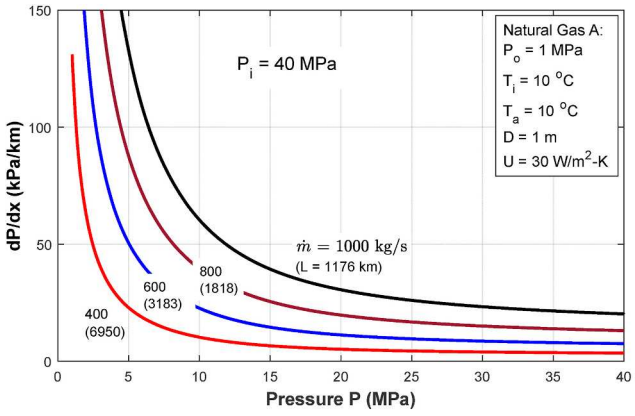

(a)

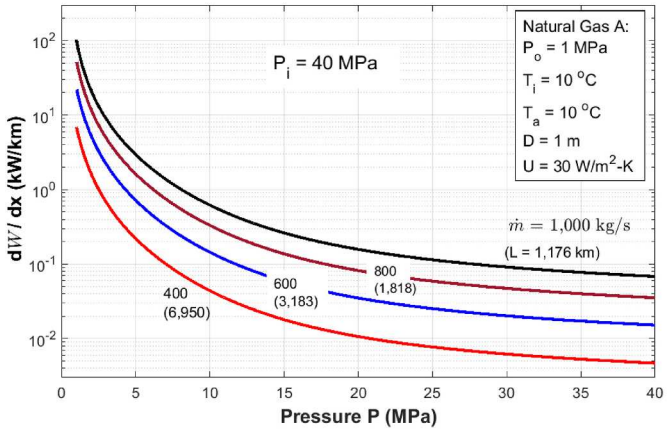

(b)

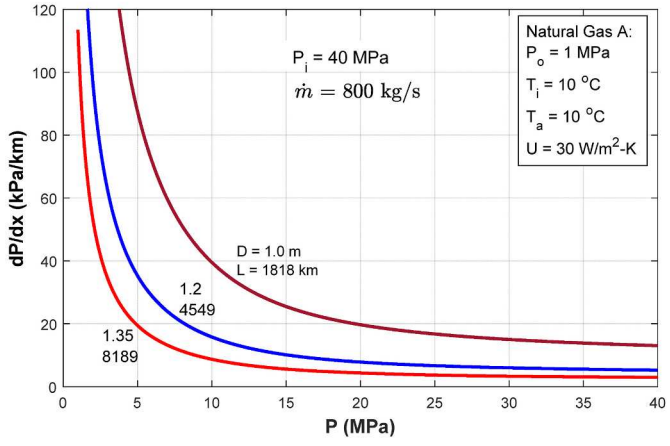

(c)

Fig. 4. Effect of: (a) mass flow rate on pressure drops per unit length, (b) mass flow rate on pumping power per unit length, and (c) diameter on the pressure gradient.

the square of the pipe diameter ($\dot{m} = \rho u \pi D^2/4$). Note that the total pressure loss is the same in each case but the density, ρ, changes with the distance, which will certainly have some effect. However, that is not the complete answer; the complex relationship between the friction factor and diameter through velocity, Eqs. 13–15, influences significantly the distance travelled for a given pressure drop. The effect of the diameter on pressure drops per unit length, dP/dx, at various pressures are presented in Fig. 4(c); the asymptotic behavior at high SC pressures is evident again. Vargas-Vera et al. (2020) has also shown a reduction in pressure drop with the increase in diameter but in a very limited range of pressure, 11.8–14.8 MPa.

Fig. 4(c) shows that the larger the diameter the lower is the pressure drop for any given P, in all regimes - subcritical gaseous to SC fluids, which is an additional advantage in the case of larger diameters. This is clearly exhibited by Fig. 5(a) where dW/dx is compared for $D = 1.2$ and 1.35 and $P_i = 30$ and 15 MPa, with P_o being 6 MPa in all cases. As can be seen, dW/dx is larger when the distance travelled is shorter, i.e., D is smaller. Indeed, the pumping power per unit length increases as the distance from the inlet increases and pressure decreases. This is consistent with Fig. 5(a), which shows larger gradient of W at lower pressure. It can also be observed in the same figure that the curves for 30 MPa has just shifted, almost horizontally, from the curves for 15 MPa, and also, that the larger the diameter the smaller is the peak value of dWW/dx.

The implication here is that in the (high) supercritical regime, the pressure drops per unit length, dP/dx, is smaller than that in the low SC regime, and much smaller than that at the subcritical states, and so is the pumping power required per unit length, dW/dx. Interestingly, when the pipeline researchers and industry think about the dense phase transport, they consider P_i greater than P_{cr}, and generally, up to 18 MPa (Baker, 2005; Moshfeghian, 2012; Vargas-Vera et al., 2020). What Fig. 4(a)–(c) are showing is that the real (huge) benefit lies beyond P_i of 15 MPa for $\dot{m} = 400$ kg/s, or slightly higher inlet pressures for higher mass flow rates. This is an *extremely important discovery* with huge implications as below.

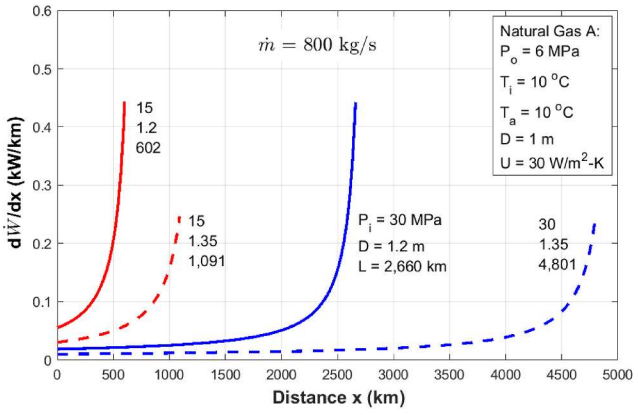

(a)

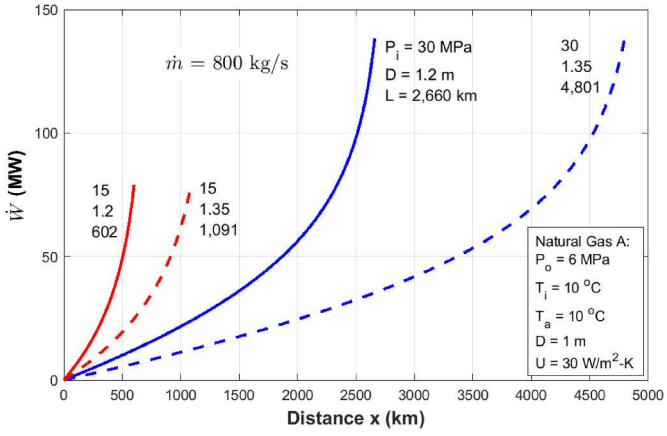

(b)

Fig. 5. Pumping power for $P_i = 15$ and 30 MPa, $D = 1.2$ and 1.35 m, and $\dot{m} = 800$ kg/s: (a) with distance from the inlet and (b) total for the length.

3.4. Power requirement and recompression advantage of SC transport

Fig. 5(a) and (b) and Tables 3–6 present the total pumping power (W) required, following Eqs. (19) and (20), from the inlet to exit. There are several conclusions that can be made here with respect to W. First, the pumping power required increases as the mass flow rate goes up for a given P_i (Table 3) and it is directly proportional. For example, when $\dot{m}$ increases from 600 to 800 to 1000 kg/s, W increases in the same proportion by about 33% and then by 24%. This is true for all inlet pressures even though the transmission distance changes significantly.

Table 4 shows that for any given P_i, the distance travelled increases significantly with the diameter but the total pumping power required changes very slightly (for 15 MPa, from 1 to 1.35 m, 2% increment), as also observed in Fig. 5(b). The most interesting part of Table 4 and Fig. 5 (b) is that as the P_i increases both the transmission distance and pumping power increase simultaneously but not in the same proportion. For example, for pipe diameter, $D = 1.2$ m, outlet pressure, $P_o = 6$ MPa, and inlet pressure, $P_i = 15$, 30, and 45 MPa, L changes from 602 km to 2660 km to 5427 km, respectively. The corresponding change in power requirement is from 79.1 MW to 138.4 MW–180.6 MW. That means, the increases in power requirement by 75% and 128% from 79.1 MW at $P_i =$ 15 lead to the increases in transmission distance by ~340% and ~800%. This is true, in almost the same proportions, for all three diameters in Table 4.

Moreover, for $\dot{m} = 800$ kg/s and $D = 1.0$ m if we use a compressor to increase power from 6 MPa to 15 MPa, then we will need more than four compressors of what one compressor would do if P_i is brought from 6 MPa to 30 MPa for the transmission of Gas A by 1060 km (Fig. 2(c)). In reality, five compressor stations would be needed if we consider the efficiencies of five compressors versus one. The ratio remains the same for all diameters in Table 5. The corresponding reduction in pumping power per 100 km is substantial.

However, if P_i can be increased to 40 MPa then that will be equivalent to 8 compressor stations with P_i of 15, and for 45 MPa it would be equivalent to 9 or 10 compressors (Table 5). As is convincingly evident that the need of compressors will go down substantially if the SNG transport is adopted, and of course, the higher the inlet pressure, the larger would be the benefit. If we consider the installation, operation, maintenance, and security of one very-large compressor station versus 5–10 large compressor stations, the saving would be enormous. If we add to this the cost of pumping power per 100 km, which decreases to ~40%, ~28%, and ~25% at 30, 40, and 45 MPa inlet pressures in comparison to 15 MPa (Table 5), the savings can further multiply. Moreover, the savings on pumping power can become further larger, if the diameter is increased, e.g., only 22.5% power required for every 100 km at $D = 1.35$ m compared to that at $D = 1$ m (Table 5).

For completeness, we have also considered the exit pressure, P_o of 1 MPa as shown in Table 6. In comparison with Table 4, the reduction in exit pressure from 6 MPa to 1 MPa requires more pumping power, e.g., an increase from 77.8 MW to 256.5 MW (compare Tables 4 and 6), a net increase of 178.7 MW for $\dot{m} = 800$ kg/s. As can be expected at all diameters and inlet pressures, this remains almost the same, about 180 MW. This represents the power required for changing the pressure from 1 to 6 MPa, which will be a function of mass flow rate but not the pipe diameter and the inlet pressure.

Table 3
Effect of mass flow rate on power requirement and transmission distance, $D =$ 1.2 m, $P_o = 6$ MPa.

$\dot{m}$ (kg/s)	P_i (MPa)		
	15	30	40
600	59.7 MW	104.2 MW	126.0 MW
	1056 km	4642 km	7744 km
800	79.1 MW	138.4 MW	167.4 MW
	602 km	2660 km	4453 km
1000	98.0 MW	172.0 MW	208.3 MW
	389 km	1722 km	2888 km

Table 4
Effect of diameter on power requirement and transmission distance, $\dot{m} = 800$ kg/s, $P_o = 6$ MPa.

D (m)	P_i (MPa)			
	15	30	40	45
1.0	77.8 MW	136.8 MW	165.7 MW	179.0 MW
	240 km	1060 km	1779 km	2172 km
1.2	79.1 MW	138.4 MW	167.4 MW	180.6 MW
	602 km	2660 km	4453 km	5427 km
1.35	79.5 MW	138.9 MW	167.9 MW	181.0 MW
	1091 km	4801 km	8014 km	9755 km

Table 5
Savings in number of compressor stations and pumping power per 100 km in comparison with $P_i = 15$ MPa corresponding to Table 4, $\dot{m} = 800$ kg/s, $P_o = 6$ MPa.

D (m)		P_i (MPa)			
		15	30	40	45
1.0	Distance, L, km	240	× 4.41	× 7.41	× 9.05
	No. of Compr.	32.4	1:5	1:8	1:10
	W/100 km, MW		× 0.4	× 0.287	× 0.254
1.2	Distance, L, km	602	× 4.42	× 7.40	× 9.01
	No. of Compr.	13.14	1:5	1:8	1:10
	W/100 km, MW		× 0.4	× 0.287	× 0.253
1.35	Distance, L, km	1091	× 4.40	× 7.35	× 8.94
	No. of Compr.	7.287	1:5	1:8	1:10
	W/100 km, MW		× 0.4	× 0.288	× 0.255

Table 6
Pumping power requirement and transmission distance when, $\dot{m} = 800$ kg/s, P_o = 1 MPa.

D (m)		P_i (MPa)		
		15	30	45
1.0	W	256.5 MW	316.3 MW	360.8 MW
	L	279 km	1060 km	2211 km
	W/100 km	91.94 MW	28.78 MW	16.32 MW
1.2	W	261.8 MW	319.8 MW	363.1 MW
	L	698 km	2756 km	5523 km
	W/100 km	37.51 MW	11.60 MW	5.52 MW
1.35	W	263.0 MW	322.1 MW	364.7 MW
	L	1266 km	4976 km	9930 km
	WW/100 km	20.77 MW	6.47 MW	3.67 MW

3.5. Effect of variation in natural gas composition

As can be expected, small changes in natural gas composition will not make much difference to the distance travelled. For example, when all parameters remain the same ($P_i = 30$ MPa, $P_o = 6$ MPa, $T_i = T_a = 10$ °C, $U = 30$ W/m^2·K, and $\varepsilon = 5$ μm) Gas B with mass flow rate of 400, 600, and 1200 kg/s will travel almost the same distance as Gas A, Fig. 2(c) and 6(a), respectively. The distance travelled by Gas C with similar parameters, is somewhat larger than that by Gas A and B when the mass flow rate is lower.This is reasonable since the compositions of Gas A and B are very similar, and that of Gas C slightly different (Table 1). However, in the case of very high mass flow rate, e.g., 1200 kg/s, this difference vanishes. Evidently, the pressure drop shows a similar pattern. Although the detailed effects of parameters considered for Gas A on temperature along the pipeline will be studied later, Fig. 6(b) is presented here to demonstrate that not only the pressure drop but also the temperature change is very similar for the three Gases A, B, and C compared here. Given this, we will mostly focus on Gas A for further parametric analysis.

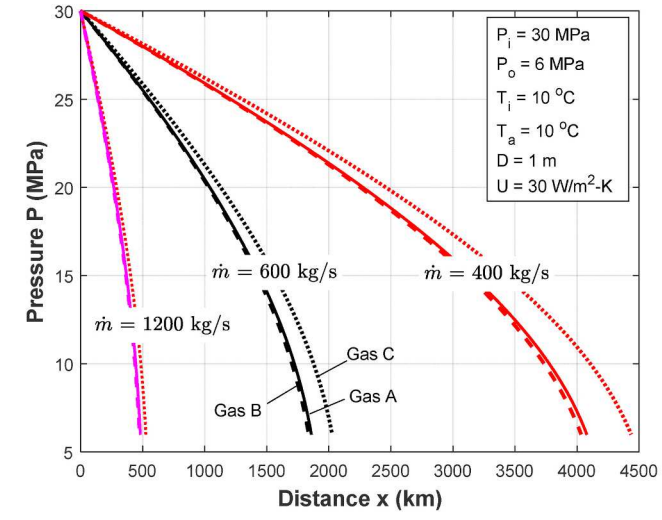

(a)

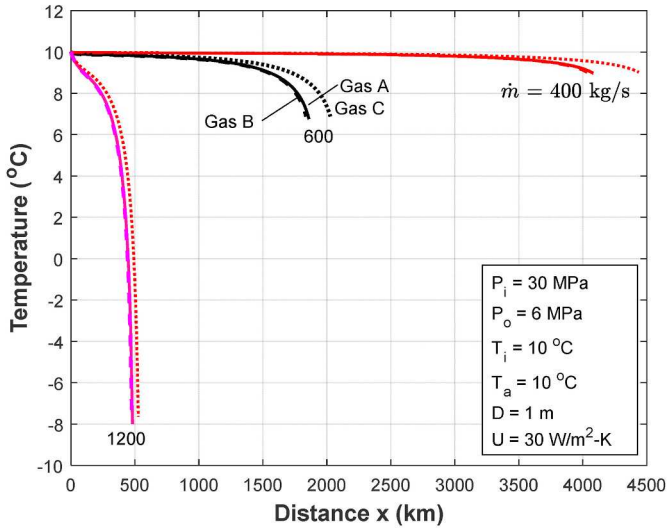

(b)

Fig. 6. Transmission distance for Gas B and C compared with Gas A for $\dot{m}$ = 400, 600, and 1200 kg/s, (a) pressure drop and (b) temperature variation.

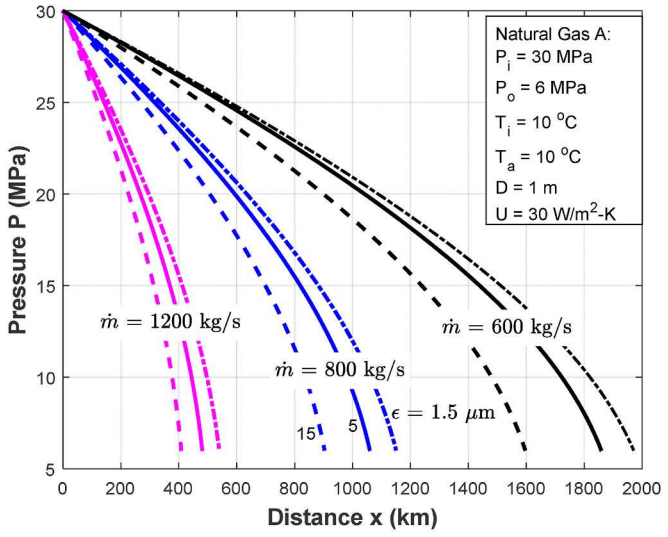

(a)

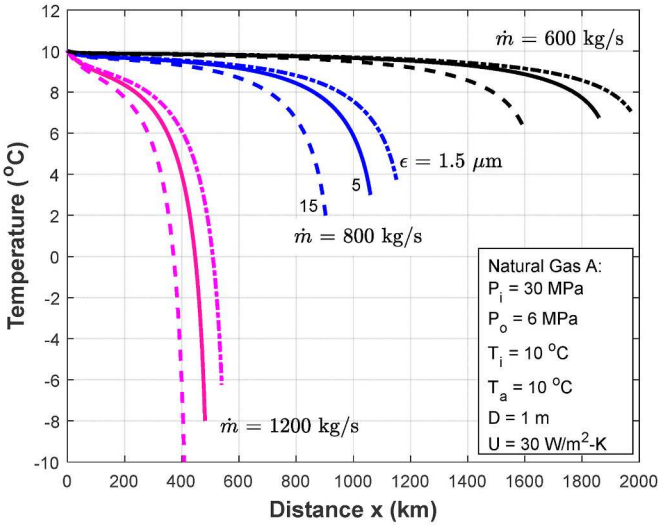

(b)

Fig. 7. Effect of surface roughness, ϵ = 1.5, 5 and 15 μm in the case of Gas A (a) pressure drop and (b) temperature variation.

3.6. *Effect of roughness*

Fig. 7(a) presents the effect of the surface roughness of $\epsilon = 1.5$, 5, 15 μm. As can be observed, the distance travelled goes down when ϵ increases, almost 25% reduction from 1.5 to 15 μm. The temperature drop also increases with the roughness, the effect being more pronounced at higher mass flow rates (Fig. 7(b)). Helgaker (2013) has provided a detailed discussion on the pipe roughness. Evidently, the roughness effect remains unchanged from subcritical to supercritical states, at all pressures.

3.7. *Joule-Thomson effect and the overall heat transfer coefficient*

Figs. 7(b) and 8 exhibit the Joule-Thomson effects on gas temperature together with the effect of overall heat transfer coefficient, U. The heat conductance, U, may include convective heat transfer at the inner and outer surfaces, conduction and convection through the soil if the pipe is buried, and conduction through the pipe wall that may consist of coatings at inner and/or outer surfaces, pipe material, and insulation.

In general, the temperature drops near the exit because of the Joule-Thomson effect that is the fluid gets colder as it expands due to a decrease in pressure (reverse of what happens when the gas is compressed). This drop in temperature is significantly higher when the heat transfer to the gas from surrounding is restricted by insulation. For example, in Fig. 8(a) for Gas C the temperature at the exit may become less than −25 °C when U is 2 W/m^2·K for the flow rate of 600 kg/s and $T_i = T_a = 0$ °C. However, the temperature drop may be only a couple of degrees if the heat conductance, U, is increased to 100 W/m^2·K, with a little impact on the distance travelled, only 88 km shorter. In addition, the distance over which the temperature reduction takes place decreases significantly as U is increased. The implication is clear that towards the end of the pipe the overall heat transfer coefficient needs to be maintained as high as possible. Note that in Fig. 8(a), we have considered Gas C to show again that the overall behavior does not change much among Gas A, B, and C; Fig. 3(b), 7(b) and 8(b), and (c) are all for Gas A.

Fig. 8(b) illustrates that the temperature drop will substantially increase if the mass flow rate is increased. As an example, for $U = 2$ W/m^2·K and $T_i = T_a = 10$ °C, the temperature drops to −18 °C (28 °C drop) for 600 kg/s and to −41 °C (51 °C drop, in the Gray Zone) with 1200 kg/

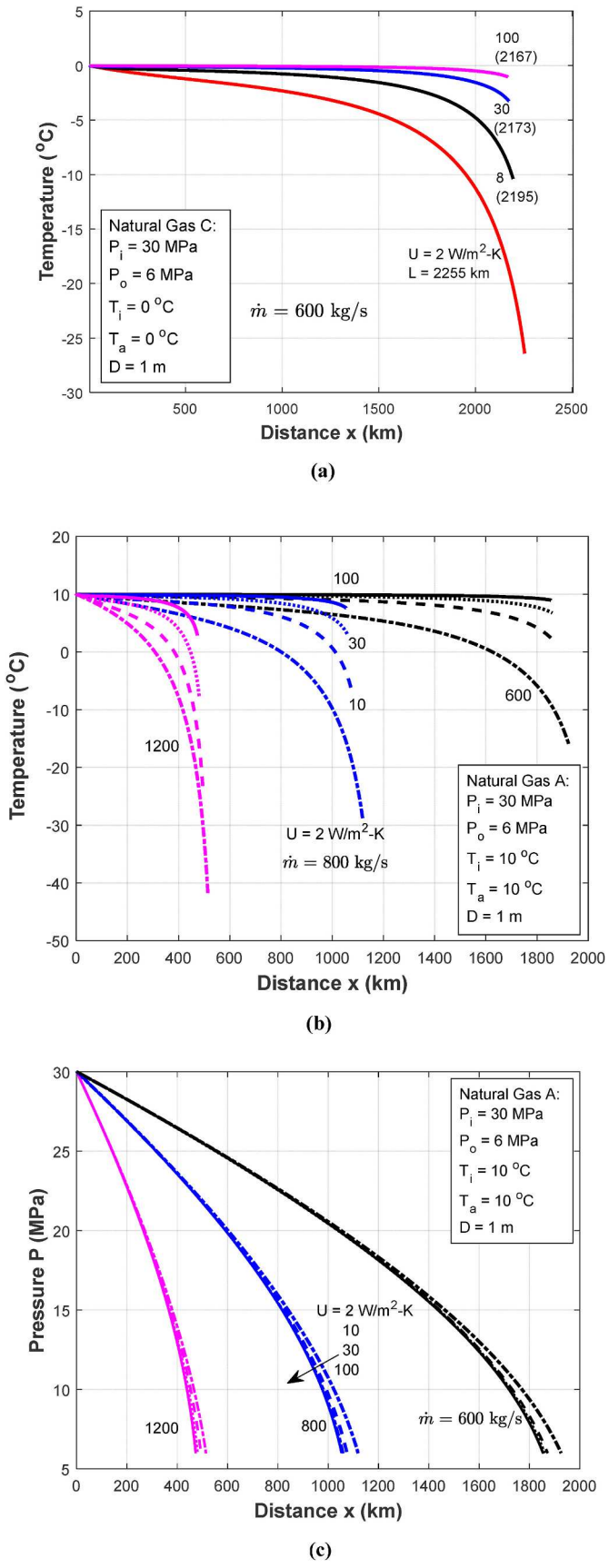

Fig. 8. Joule-Thomson effect as a function of overall heat transfer coefficient (heat conductance), $U = 2$, 10, 30 W/m^2·K for (a) temperature drop for Gas C with $\dot{m} = 600$ kg/s, (b) temperature drop for Gas A with $\dot{m} = 600$, 800, 1200 kg/s, and (c) pressure drop for Gas A, with $\dot{m} = 600$, 800, 1200 kg/s.

s. Again, this drop can be reduced if U is increased, i.e., the thermal resistance is reduced significantly.

Fig. 3(a2)-(c2) demonstrates very similar drops in temperature with the reduction in diameter, for a given mass flow rate. The implication here is that the larger the distance travelled by SC natural gas because either the mass flow rate is low or the diameter is large, the smaller is the Joule-Thomson effect, and as a result, the smaller is the temperature drop in the exit region. Indeed, Fig. 8(b) shows lower temperature drop at $U = 30$ W/m^2·K and much lower drop at 100 W/m^2·K, in all cases. However, as seen in Fig. 8(c) the effect of U on the rate of pressure drop is minimal. Therefore, it can be concluded that if the gas is delivered to a place in the warmer region, it may be advisable to let the gas gain heat from the surrounding to balance the temperature drop towards the end of the pipe. Alternatively, in some cases, the gas may require to be actively heated.

3.8. *Effect of surrounding temperature*

As shown in Fig. 9(a), the distance travelled increases significantly as the surrounding temperature, T_a, decreases, e.g., from 938 km to 1431 km (53% increase) when the temperature goes down from 30 °C to −30 °C. Even if the temperature is lowered less, from 15 °C to −15 °C, the distance travelled for the same pressure loss increases by 23%. Similar increase in the distance travelled as temperature decreases has also been reported by Zivdar and Abofarakh (2021). From Fig. 9(a), it is also evident that the temperature of the gas ($T_i = 5$ °C) changes very fast and comes closer to the ambient temperature, T_a, within a short distance since U is sufficiently high, 30 W/m^2·K. As expected, there is a slight drop in gas temperature near the exit because of the Joule-Thomson effect.

Strikingly different temperature profile is observed in Fig. 9(b) when U is decreased from 30 to 2 W/m^2·K, i.e., the thermal resistance is significantly increased, although the distance travelled does not change much (compare with Fig. 9(a)). Indeed, the near isothermal condition for most part in Fig. 9(a) is replaced by large variations in temperature. For $T_a = 30$ °C, the gas temperature, T_x, first increases because of the heat generated by viscous dissipation as well as the surrounding temperature being high (heat gain), and then decreases to a lower temperature because of the Joule-Thomson effect (Fig. 9(b)). The effect diminishes as T_a decreases and at $T_a = 0$ °C, T_x does not go above T_i. Indeed, in the case of $T_a = -30$ °C, it goes close to the cricondentherm, T_{cr} (Fig. 9(c)); this does not happen when $U = 30$ W/m^2·K.

The above findings have many implications with respect to the geographic locations, climatic conditions, pipe insulation, and the lowest temperature that can keep the gas outside the anomalous state, as follows:

a. The gas temperature should not go below the value that is required to keep it outside the anomalous state; this minimum temperature, however, is a function of pressure as discussed in Section 3.1, and also, in Almara et al. (2023).
b. The insulation is not advantageous in the cold region unless required by the condition in (a). If the circular pipe is covered by a square cross section concrete as is practiced in many situations, efforts should be made to increase the radial heat transfer from gas by reinforcing concrete with metal rods radially.
c. In the cold region, the depth of the underground pipe should be appropriately selected to keep the gas at the lowest possible temperature within the constraint of (a). Moreover, in many places, it may be advisable to keep the pipe just exposed to the ambient.
d. In the warmer region, the pipe should be placed underground as deep as possible to maintain the gas at a lower temperature, and a balance could be achieved among the friction heating of the gas, heat gain from or loss to the surrounding, and variation in the ground temperature because of solar radiation. However, this needs to be analyzed carefully in light of the findings in Sections 3.7 and 3.8.

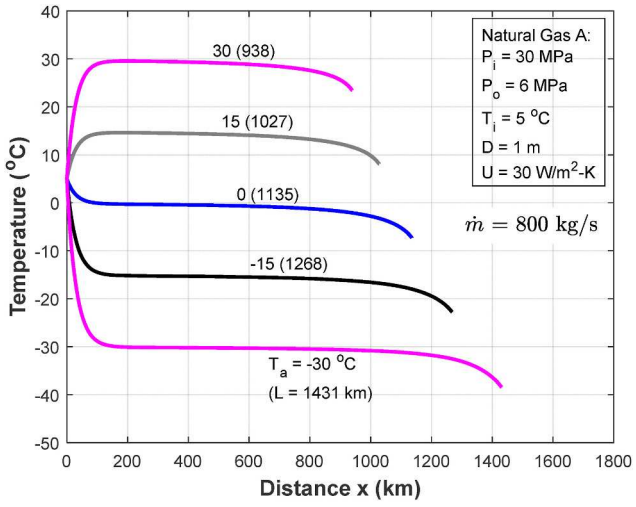

(a)

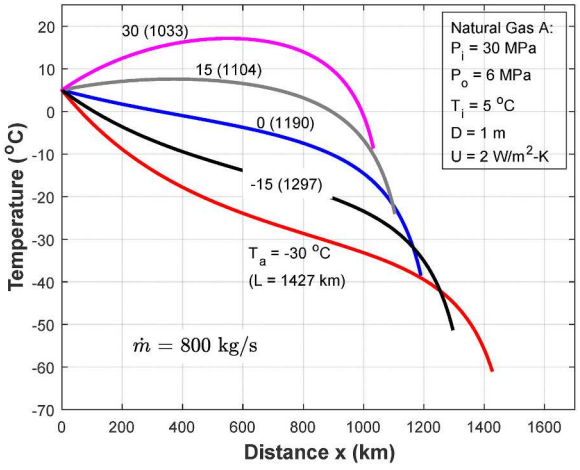

(b)

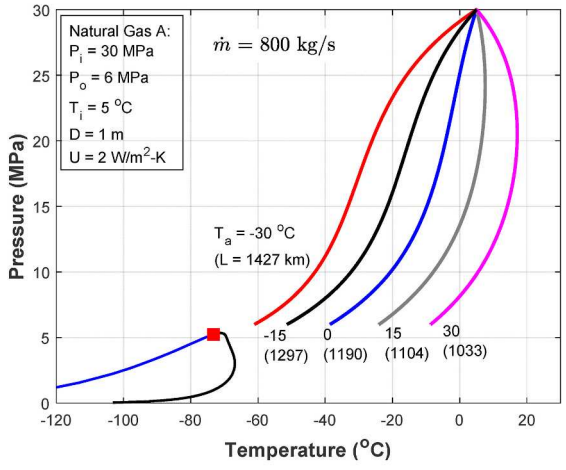

(c)

Fig. 9. Temperature variation along the pipe for Gas A, for a range of surrounding/ambient temperature, $T_a = -30, -15, 0, 15, 30$ °C when the inlet temperature, $T_i = 5$ °C, $\dot{m} = 800$ kg/s, and heat transfer coefficient of the pipe, (a) $U = 30$ W/m^2·K, (b) $U = 2$ W/m^2·K, and (c) against the pressure for $U = 2$ W/m^2·K.

e. When crossing large water bodies and/or ocean, it would be beneficial to lay the pipe at the bottom to take advantage of the lowest temperature there. Indeed, in the case of ocean and large water bodies, this would yield an almost isothermal flow at the water (bottom) temperature since the heat capacity of surrounding water would be high.
f. In case it is impossible to control the gas temperature from going down into the anomalous state of the gas, say below −30 °C, it may be desirable to bring the T_c and T_{cr} down by enriching the gas with methane or by adding nitrogen or argon, both of which have much lower critical temperatures (Prasad et al., 2022b; Almara et al., 2023).

3.9. Pipeline transport through the ocean and large water bodies

As is evident from the above results: (a) an isothermal gas flow condition is better, (b) a lower surrounding temperature, T_a, is more desirable, (c) if $T_a < T_x$, a higher overall heat transfer coefficient is more appropriate, and (d) a surrounding environment of high heat absorbing capacity with negligible change in its temperature is more advantageous. Obviously, large water bodies, particularly oceans, meet all of these sought-after conditions.

Here, we present a case study of the pipeline transport through ocean bottom by considering the water temperature, $T_a = 4$ °C and overall heat transfer coefficient, U, as 100 W/m^2·K which implies almost no resistance to heat flow in or out (Fig. 10). In the case of 1.2 m diameter pipe, mass flow rate of 600 kg/s, and pressure drop of 30 to 6 MPa, the gas can travel to a distance of 4823 km (Fig. 10(a)) compared to 4642 km when $T_i = T_a = 10$ °C and $U = 30$ W/m^2·K (Fig. 3(a1)).

Fig. 10(b) reveals the major advantage of the pipelines at ocean

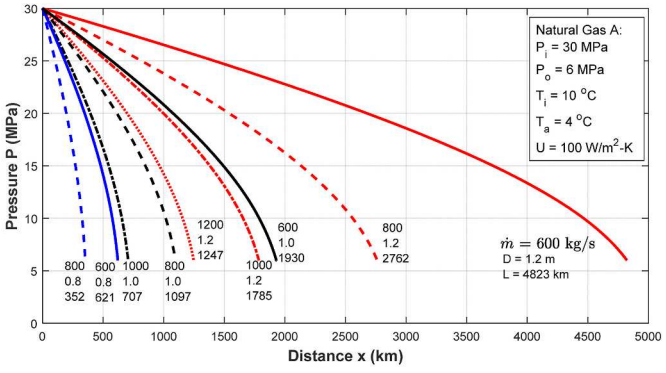

(a)

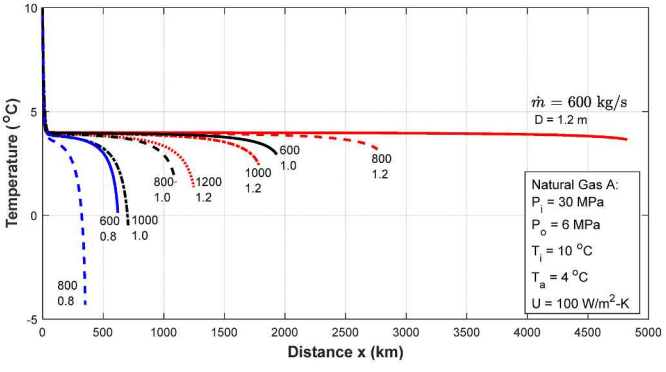

(b)

Fig. 10. Transmission of Gas A at the ocean bottom, $T_a = 4$ °C with inlet temperature, $T_i = 10$ °C, and heat conductance of the pipe, $U = 100$ W/m^2·K: (a) distance and pressure drop, and (b) temperature variation (—— 600 kg/s,- - - - 800 kg/s,—·—·— 1000 kg/s,····· 1,200 kg/s).

bottom, i.e., almost isothermal flow conditions. As seen, the temperature drops very quickly from 10 °C to 4 °C, and remains there for almost the entire length, when $D = 1.2$ m and $\dot{m} = 600$ kg/s. However, an increase in mass flow rate does show a small drop in gas temperature in the end zone, which increases as $\dot{m}$ is increased. This effect enhances significantly when the pipe diameter is reduced; the temperature drops by 8 °C below the water temperature when $D = 0.8$ m and $\dot{m} = 800$ kg/s. However, these increases in the end zone temperature are still small and can be easily handled.

3.10. Some salient features of pipelines at the ocean bottom

In the case of pipeline laid down at the ocean bottom, it would be beneficial to install a compressor station near the coastline from where the ocean pipeline starts. This may facilitate longer pipeline transport without the need of recompression under the ocean. Indeed, the compressor installed at the coastline will not need an active cooling system to bring the gas temperature down after compression; cooling can be achieved by using the ocean water.

With the SNG pipeline at ocean bottom, there may not be any need of recompression in most situations. However, if the recompression is required, particularly when the gas has to be delivered at ultra-high mass flow rates at locations far away from the extraction or processing facilities, one or more compressor stations may be installed, as is the current practice.

The first choice would be then to place compressor stations on islands, if they exist between the coastlines of the supply side and the delivery point, and are available for this purpose. If no islands are available, there can be two possible options: (a) a submerged (submarine) compressor, or (b) a compressor housed on a floating platform. Although there are challenges with both of these options, the technology of floating platform is well developed. In this case, the pipe will need to be brought up from the bottom and then after recompression taken down. In such an arrangement, the negative effects of gravity in bringing the gas up would be balanced by the positive effects of gravity when the gas flows down. The additional operational cost will be basically due to the pressure loss caused by the added length of the pipe, equivalent to a few kilometers. On the other hand, the submarine technology is also reasonably matured and can be developed further to meet the needs of the ocean pipelines.

3.11. Regional/local distribution

After the above analysis and discussions, an obvious question is, can we continue with the gas transport regionally or locally since the exit pressure, ~6 MPa, is still much above the pressure at which the gas is delivered to industrial and residential consumers. The simple answer is yes! However, it will depend on the temperature at the exit as well as on how far are the consumers from delivery point. Obviously, if the consumers are far away, then recompression(s) may be needed at select location(s).

With respect to the exit temperature, Fig. 11(a)-(c) shows that the exit temperature (SC pipeline), T_o for Gas A is above the cricondentherm, T_{cr}, for all mass flow rates, 400–1200 kg/s and pipe diameters of 1.0, 1.2, and 1.35 m. If this gas continues to flow to a lower pressure, e.g., the atmospheric pressure, ~0.1 MPa, the temperature may come down to a value between ~7 °C and – 60 °C, which is still above the cricondentherm, T_{cr}. However, this does not guarantee that the exit temperature would be beyond the anomalous state, particularly in the case of mass flow rate of 800 kg/s and up, with $D = 1.0$ m. Note that there exists anomalous region even under the subcritical gaseous states (Prasad et al., 2022a, 2023). Fortuitously, a simple solution to this problem is just heating the gas either passively if the ambient temperature is high, or actively if the ambient conditions do not allow that. In all other cases in Fig. 11, the temperature is in the safe zone.

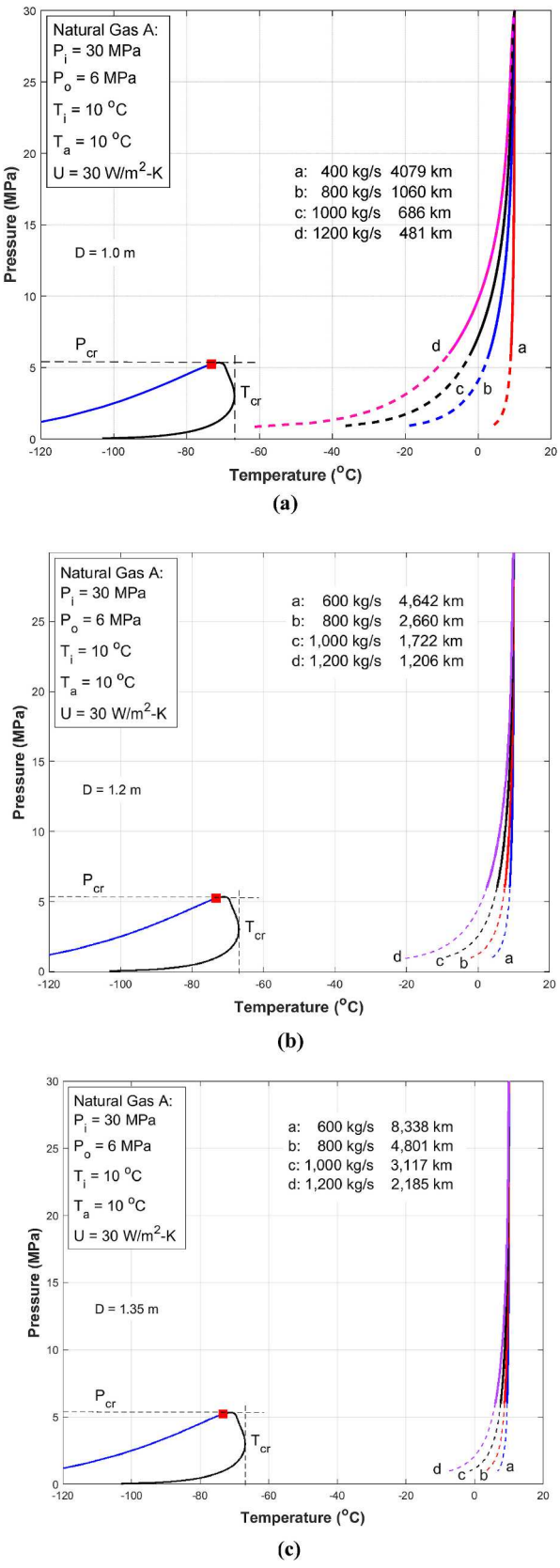

Fig. 11. Regional/local distribution of Natural Gas A without recompression at delivery point, with $\dot{m} = 400$–1200 kg/s, (a) $D = 1.0$ m, (b) $D = 1.2$ m, and (c) $D = 1.35$ m.

3.12. Transport of natural gas extracted from wells to processing facilities

Another follow up question is, can SNG transport method be used to bring the extracted gases from wells to the processing facilities which are remote, e.g., in the case of offshore drilling or extraction in the polar region. (Generally, the hazardous constituents are taken out and/or the gas is enriched by adding high calorific value hydrocarbons at the processing facilities). The answer is again yes! In such situations, the requirement of the delimitation of the anomalous region can be met by a theoretical analysis provided the constituents and their fractions in the gas coming out of the well are known. Alternatively, an experimental approach may be adopted to develop a pressure-temperature line to delimit the anomalous state on the supercritical side.

3.13. Transport of gases from methane hydrates

Methane extracted from methane hydrates in the sediments at ocean bottom (research still under progress) can be transported to the ocean surface or nearest coastline using the proposed SNG transport method. It is expected that the extracted methane will already be under supercritical conditions. In addition, the SNG method can also be used to transport natural gas from the storage of solidified natural gas (Hassanpouryouzband et al., 2020).

4. Concluding remarks

As reported (Almara et al., 2023), supercritical pressure, $P \geq 6$ MPa and temperature, $T > -30$ °C, may be considered as the safe zone and $P \geq 6$ MPa and temperature, -50 °C $< T < -30$ °C, as a gray area, which will require special design considerations for the SNG pipeline transport. This observation is based on the average compositions of natural gas from US/Canada (Gas A), West Asia (Gas B), and North Sea (Gas C). Following conclusions are then derived from the results presented here:

- Supercritical natural gas can travel ultra-long distances without recompression, far beyond what has been commercially achieved or proposed thus far. This delivery distance strongly depends on the inlet pressure, mass flow rate, and pipe diameter. Indeed, the travel distance increases significantly with the inlet pressure and pipe diameter, but decreases with the mass flow rate and surface roughness.
- In SNG pipeline transport, the pressure loss per unit length would decrease substantially as the supercritical pressure increases beyond 6 MPa, and would finally achieve asymptotic (low) values at pressures above 15 MPa. Indeed, more than an order-of-magnitude reduction in the pressure loss is possible.
- The pumping power (per unit length) required for SNG transport decreases considerably with the increase in the inlet pressure, beyond 15 MPa. As a result, the higher the inlet pressure, the lower would be the total pumping power.
- Also, the power required per 100 km transport of SNG decreases significantly as the pipe diameter is increased for any given inlet pressure.
- Consequently, it is possible to completely eliminate the compressor station(s) between the inlet and exit of the pipeline and build highly-energy-efficient natural gas pipeline systems.
- The flow phenomena and pumping power requirements in the high-pressure supercritical regime are, therefore, much different from that in the regimes of low pressure and mid-pressure (dense phase as considered thus far), e.g., from 15 MPa to 3–5 MPa.
- The larger the mass flow rate, the smaller the pipe diameter, and/or the higher the thermal resistance between the gas and the surrounding, the stronger is the Joule-Thomson effect, i.e., the drop in temperature near the exit.
- The pressure loss decreases and the delivery distance increases with decreasing gas temperature. Hence, it is desirable to keep the temperature of the gas in transit as low as possible. This implies that: (i) the pipes to transport SNG in cold regions, including arctic, should allow the heat loss to surrounding as much as possible, (ii) the pipes carrying gas from a cold region to a warm region be insulated as best and as long as possible, and (iii) the buried SNG pipeline is preferable in the warmer regions.
- The isothermal condition, ~4 °C, at the bottom of the ocean with infinite heat capacity provides the best condition for SNG transport. Needless to mention that in many cases cross-country pipelines under ocean will be much shorter than that passing over the land.
- Another advantage of SNG transport is that immediate recompression for local/regional distribution may not be needed at the delivery point since the exit pressure would be about 6 MPa or more. If the exit temperature is near cricondentherm, the gas may need heating.

A chart, as presented in Fig. 12, shows the sequence of input parameters/considerations in their approximate order of importance to achieve the goals for ultra-long distance, very-high mass flow rates, minimal/no recompression stations, and energy-efficient transport of natural gas.

In this paper, we have revealed the enormous possibility of transport of natural gas without liquefaction to far-distant destinations/countries

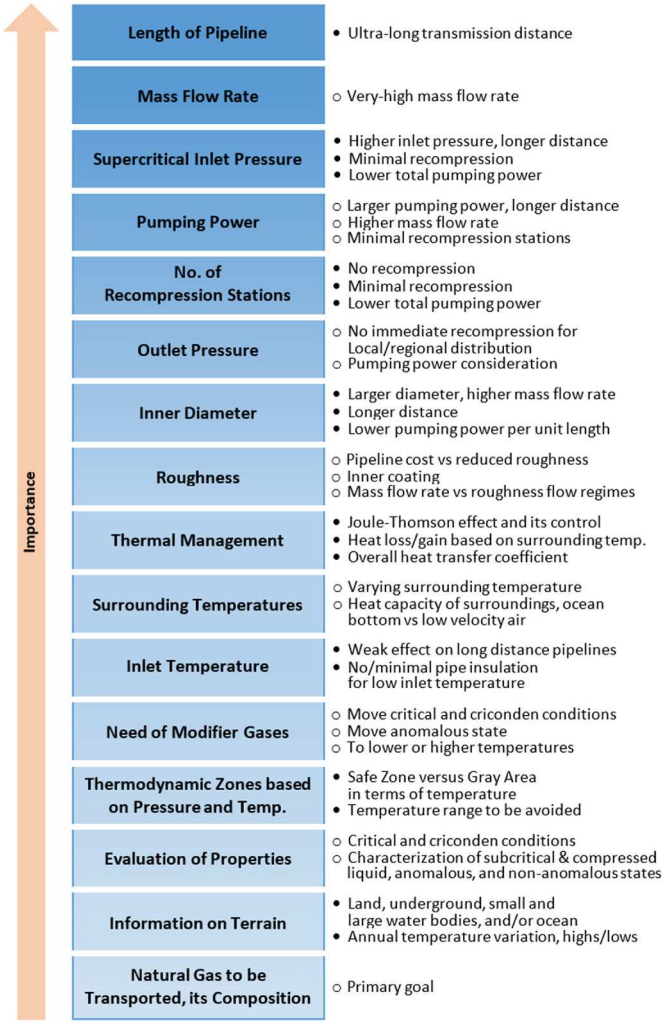

Fig. 12. Chart, showing the sequence of input parameters/considerations in their approximate order of importance for ultra-long distances, very-high mass flow rates, minimal/no recompression stations, and energy-efficient pipeline transport.

that has not been achieved thus far. We are cognizant of the materials, design, manufacturing, and construction constraints, which the benefits of this innovative approach can certainly overcome. With SNG transport via under-ocean pipelines, it would be possible to directly connect the island countries with the producer countries. Indeed, a look at the world map reveals many possibilities of SNG transport from the producer countries to consumer countries either directly without recompression or via islands that can serve as rentier states for recompression stations. Alternatively, recompression stations either submerged in the ocean or on floating platforms can serve this purpose. We believe the SNG transport can greatly help in worldwide energy security.

Funding

The first and second authors (VP, LA) were partially supported by US National Science Foundation Award No. 2231393.

Author contributions

Vish Prasad, Conceived and designed the analysis, Performed the analysis, Wrote the paper, **Laura M. Almara**, Collected the data, Performed the analysis, **Guo-Xiang Wang**, Conceived and designed the analysis, Contributed data or analysis tools, Performed the analysis, Wrote the paper

Declaration of competing interest

The authors declare that they have no known competing financial interests or personal relationships that could have appeared to influence the work reported in this paper.

Data availability

Data will be made available on request.

Acronyms and Notations

Symbols

B	Mass flow parameter, Eq. (8)
c_v	Specific heat at constant volume, J/(kg^{-1}·K^{-1})
dr	Draught factor, Eq. (16)
D	Diameter, m
f	Friction factor
g	Gravity, m/s^2
K	Coefficient, Eqs. (17) and (18)
L	Transmission length, m
$\dot{m}$	Mass flow rate, kg/s
M	Molecular weight, kg/kmol
n	exponent
P	Pressure, Pa, MPa
P_{cr}	Cricondenbar, Pa, MPa
$q^{'}$	Rate of heat transfer per unit length of pipe, W/m
Re	Reynolds number
T	Temperature, °C, K
T_{cr}	Cricondentherm, °C, K
T_x	Local gas temperature inside the pipe, °C, K
u	Flow velocity in x-direction, m/s
U	Total heat transfer coefficient, W/(m^2·K)
W	Pumping power, W, MW
x	Direction of pipeline, horizontal
X	Coefficient, Eq. (18)
Y	Coefficient, Eq. (18)
z_i	Gas composition

Greek Symbols

β	Isobaric coefficient of volumetric expansion, K^{-1}
ε	Surface roughness of the pipe, m
θ	Angle with horizontal, degrees
κ	Isothermal compressibility, Pa^{-1}
μ	Dynamic viscosity, N·s·m^{-2}, Pa·s
ρ	Density, kg·m^{-3}
τ	Wall shear stress, Pa

Subscript

a	Ambient, surrounding
c	Value at critical point
cr	Value at criconden condition
i	Inlet
o	Outlet
P	Derivative at constant pressure
T	Derivative at constant temperature

w	Wall
r	Reduced
ρ	Derivative at constant density

Abbreviations

1D	One dimension
3D	Three dimension
C1	Methane, CH_4
C2	Ethane, C_2H_6
C3	Propane, C_3H_8
i-C4	i-Butane, C_4H_{10}
n-C4	n-Butane, C_4H_{10}
i-C5	i-Pentane, C_5H_{12}
n-C5	n-Pentane, C_5H_{12}
EOS	Equation of State
GERG	European Gas Research Group
LNG	Liquefied Natural Gas
NS	Nord Stream
PR	Peng-Robinson
SC	Supercritical
SNG	Supercritical Natural Gas

References

Abdolahi, F., Mesbah, A., Boozarjomehry, R.B., Svrcek, W.Y., 2007. The effect of major parameters on simulation results of gas pipelines. Int. J. Mech. Sci. 49 (8), 989–1000. https://doi.org/10.1016/j.ijmecsci.2006.12.001.

Almara, L.M., Wang, G.X., Prasad, V., 2023. Conditions and thermophysical properties for transport of hydrocarbons and natural gas at high pressures: Dense phase and anomalous supercritical state. J. Nat. Gas Sci. Eng., 205072

Baker, M., 2005. Transport of North Slope Natural Gas Tidewater. Alaska Natural Gas Development Authority.

Beaubouef, B., 2011. Nord stream completes the world's longest subsea pipeline. Offshore 30. https://www.offshore-mag.com/business-briefs/equipment/engineering/article/16755095/nord-stream-completes-worlds-longest-subsea-pipeline. (Accessed 5 January 2023).

Chaczykowski, M., 2009. Sensitivity of pipeline gas flow model to the selection of the equation of state. Chem. Eng. Res. Des. 87 (12), 1596–1603. https://doi.org/10.1016/j.cherd.2009.06.008.

Chaczykowski, M., 2010. Transient flow in natural gas pipeline - the effect of pipeline thermal model. Appl. Math. Model. 34 (4), 1051–1067. https://doi.org/10.1016/j.apm.2009.07.017.

Chestney, N., 2022. Global LNG demand expected to almost double by 2040. Shell LNG Outklook. https://www.shell.com/energy-and-innovation/natural-gas. (Accessed 9 January 2023).

Corbett, K.T., Bowen, R.R., Petersen, C.W., 2004. High-strength steel pipeline economics. Int. J. Offshore Polar Eng. 14 (1), 1053–5381, 75-80.

Coulter, D.M., Bardon, M.F., 1979. Revised equation improves flowing gas temperature prediction. Oil Gas J. 107–108.

Goldwater, M.H., Fincham, A.E., 1981. Modelling of gas supply systems. In: Nicholson, H. (Ed.), Modelling of Dynamic Systems 2, fifth ed. Institute of Electrical Engineers, p. 150.

Hassanpouryouzband, A., Joonaki, E., Farahani, M.V., Takeya, S., Ruppel, C., Yang, J., English, N.J., Schicks, J.M., Edlmann, K., Mehrabian, H., Zachary, M., Aman, Z.M., Tohidi, B., 2020. Gas hydrate in sustainable chemistry. Chem. Soc. Rev. 49, 5225–5309. https://doi.org/10.1039/C8CS00989A.

Helgaker, J.F., 2013. Modeling Transient Low in Long Distance Offshore Natural Gas Pipelines. Doctoral thesis, Dept. Energy and Processes Eng., Norwegian Univ. of Science and Technology (NTNU), Trondheim Norway.

Helgaker, J.F., Oosterkamp, A., Langelandsvik, L.I., Ytrehus, T., 2014a. Validation of 1D flow model for high pressure offshore natural gas pipelines. J. Nat. Gas Sci. Eng. 16, 44–56. https://doi.org/10.1016/j.jngse.2013.11.001.

Helgaker, J.F., Muller, B., Ytrehus, T., 2014b. Transient flow in natural gas pipelines using implicit finite difference schemes. J. Offshore Mech. Arctic Eng. 136 (3), 031701 https://doi.org/10.1115/1.4026848.

Issa, R.I., Spalding, D.B., 1972. Unsteady one-dimensional compressible frictional flow with heat transfer. J. Mech. Eng. Sci. 14 (6), 365–369. https://doi.org/10.1243/JMES_JOUR_1972_014_045_02.

Katz, D.L.V., King, G.G., 1970. Dense Phase Transmission of Natural Gas. Canadian Arctic Gas Pipeline Ltd.

King, G., 1991. Ultra-high pressure Arctic natural gas pipelines. In: Proceedings of Canadian Petroleum Association, Pipeline Conference. Calgary Alberta Canada, pp. 14–16.

King, G., 1992. Ultra-high gas pressure pipelines offer advantages for Arctic service. Oil Gas J. 90, 79–84.

King, G., Kedge, C., Zhou, X., Matuszkiewicz, A., 2002. Superhigh dense phase Arctic pipelines increase reliability and reduce costs. In: Proceedings of iPC'02, 4th Int. Pipeline Conference 2002, pp. IPC2002–27302.

Langelandsvik, L.I., 2008. Modeling of Natural Gas Transport and Friction Factor for Large-Scale Pipelines. Dep. Of Energy and Process Eng.. Norwegian Univ. of Science and Technology (NTNU), Trondheim Norway. Doctoral Thesis.

Langelandsvik, L.I., Kunkel, G.J., Smits, A.J., 2008. Flow in a commercial steel pipe. J. Fluid Mech. 595, 323–339. https://doi.org/10.1017/S0022112007009305.

Lee, A., Gonzalez, M., Eakin, B., 1966. The viscosity of natural gases. J. Petrol. Technol. 18, 997–1000. SPE-Paper-1340-PA.

MacLaren, J.F.T., Tramschek, A.B., Sanjines, A., Pastrana, O.F., 1975. A comparison of numerical solutions of the unsteady flow equations applied to reciprocating compressor systems. J. Mech. Eng. Sci. 17 (5), 271–279. https://doi.org/10.1243/JMES_JOUR_1975_017_039_02.

Lemmon, E.W., Bell, I.H., Huber, M.L., McLinden, M.O., 2018. NIST Standard Reference Database 23: Reference Fluid Thermodynamic and Transport Properties-REFPROP, Version 10.0.

Material-properties.org, 2023. Austenitic Stainless Steel. https://material-properties.org/what-is-austenitic-stainless-steel-definition. (Accessed 13 March 2023).

Mazurek, D.M., Anderson, P.S., 1994. Application of Ultra-high Pressure Dense Phase Pipelines to Large Diameter Transmission Systems. NOVA Gas Int. Seminars, Kuala Lumpur, Malaysia.

Mokhatab, S., Poe, W.A., Mak, J.Y., 2019. Handbook of Natural Gas Transmission and Processing-Principles and Practices, fourth ed. Elsevier, Inc. (Chapter 1). ISBN: 978-0-12-815817-3.

Molnar, G., 2022. Economics of gas transportation by pipeline and LNG. In: Hafner, M., Luciani, G. (Eds.), The Palgrave Handbook of Int. Energy Economics, pp. 23–57.

Moshfeghian, M., 2012. Transportation of natural gas in dense phase. PetroSkills. http://www.jmcampbell.com/tip-of-the-month/2012/08/transportation-of-natural-gas-in-dense-phase/. (Accessed 5 March 2023).

Moshfeghian, M., Rajani, J., Snow-McGregor, J., 2022. Transportation of natural gas in dense phase – Nord Stream 1. https://www.petroskills.com/en/blog/entry/april2022-totm-Transportation-of-Natural-Gas-in-Dense-Phase%E2%80%93Nord-Stream-1. (Accessed 14 April 2023).

NaturalGas.Org, 2013. The transportation of natural gas. http://naturalgas.org/naturalgas/transport/. (Accessed 23 March 2023).

Osiadacz, A.J., Chaczykowski, M., 2001. Comparison of isothermal and non-isothermal pipeline gas flow models. Chemical Eng. J. 81 (1–3), 41–51. https://doi.org/10.1016/S1385-8947(00)00194-7.

Ouyang, L.B., Aziz, K., 1996. Steady-state gas flow in pipes. J. Petrol. Sci. Eng. 14 (3–4), 137–158. https://doi.org/10.1016/0920-4105(95)00042-9.

Peng, D.-Y., Robinson, D.B., 1976. A new two-constant equation of state. Ind. Eng. Chem. Fundam. 15 (1), 59–64. https://doi.org/10.1021/i160057a011.

Prasad, V., Kakroo, K., Banerjee, D., 2022a. Existence of supercritical 'liquid-like' state in subcritical region, optimal heat transfer enhancement, and argon as a non-reacting, non-corroding SC heat transfer fluid. Heat Tran. Res. 53 (9), 1–27. https://doi.org/10.1615/HeatTransRes.2022043095.

Prasad, V., Zhang, Z., Wang, G.X., Banerjee, D., Sadat, H., Bostanci, H., Almara, L.M., 2022b. Process and System for Heat Exchange Process, Patent Application No. 18/320,727, May 19, 2023. In: based on "Method and system for supercritical working fluid mixtures prepared selectively for heat dissipation at very-low to very-high temperatures." Provisional Patent, Application No 63/344, 429, May 2022.

Prasad, V., Wang, G.X., Banerjee, John, H., Bostanci, H., Sadat, H., Almara, L., 2022c. Method and Conditions for Intra- and Inter-Continental Transport of Supercritical Natural Gas (SNG) via Pipelines through Land, Underground, Water Bodies, and/or

Ocean. In: Provisional Patent, Application No. 63/375,085 (09/09/2022), Patent Application being submitted.
Ramsen, J., Losnegård, S.E., Langelandsvik, L.I., Simonsen, A.J., Postvoll, W., 2009. Important aspects of gas temperature modeling in long subsea pipelines. In: Proceedings to PSIG 0901. PSIG Annual Meeting, Galveston Texas.
Schorre, C.E., 1954. Here's how to calculate flow temperature in a gas pipeline. Oil Gas J. 66–68.
Sletfjerding, E., Gudmundsson, J., Sjoeen, K., 1998. Flow experiments with high pressure natural gas in coated and plain pipes: comparison of transport capacity. In: Proceedings to PSIG Annual Meeting Denver Colorado. Paper Number: PSIG-9808.
Thorley, A.R.D., Tiley, C.H., 1987. Unsteady and transient flow of compressible fluids in pipelines - a review of theoretical and some experimental studies. Int. J. Heat Fluid Flow 8 (1), 3–15. https://doi.org/10.1016/0142-727X(87)90044-0.
van Deen, J.K., Reintsema, S.R., 1983. Modeling of high-pressure gas transmission lines. Appl. Math. Model. 7 (4), 268–273. https://doi.org/10.1016/0307-904X(83)90080-X.
Vargas-Vera, B.H., Rada-Santaigo, A.M., Cabarcas-Simanacas, M.E., 2020. Gas transport at dense phase conditions for the development of deepwater fields in the Colombian Caribbean Sea. Ciencia, Tecnologia y Futuro 10, 17–32. https://doi.org/10.29047/01225383.131.
Wang, X., Economides, M., 2009. Advanced Natural Gas Engineering, first ed. Gulf Publishing Company, Houston, Texas. 9781933762388.
Witek, M., 2015. Possibilities of using X80, X100, X120 high-strength steels for onshore gas transmission pipelines. J. Natural Gas Sci. Eng. 27 (1), 374–384. https://doi.org/10.1016/j.jngse.2015.08.074.
Yoo, J.-Y., Ahn, S.-S., Seo, D.H., Song, W.-H., Kang, K.-B., 2011. New development of high grade X80 to X120 pipeline steels. Mater. Manuf. Process. 26 (1), 154–160. https://doi.org/10.1080/10426910903202534.
Zivdar, M., Abofarakh, M., 2021. Natural gas transmission in dense phase mode. J. of Gas Technology 6 (2), 45–52.